2364 J. Med. Chem. 2010, 53, 2364–2375
DOI: 10.1021/jm901265h

Journal of Medicinal Chemistry Article

Synthesis, Biological Activity, and Molecular Modeling Studies of 1*H*-1,2,3-Triazole Derivatives of Carbohydrates as α-Glucosidases Inhibitors

Sabrina B. Ferreira,[∥,†] Ana C. R. Sodero,[‡] Mariana F. C. Cardoso,[∥] Emerson S. Lima,[§] Carlos R. Kaiser,[†] Floriano P. Silva, Jr.,[‡] and Vitor F. Ferreira*[,∥]

[†]*Instituto de Química, Universidade Federal do Rio de Janeiro, LABRMN, Ilha do Fundão, 21949-900, Rio de Janeiro, RJ, Brazil,* [‡]*Laboratório de Bioquímica de Proteínas e Peptídeos, Fundação Oswaldo Cruz, Instituto Oswaldo Cruz, 21045-900, Rio de Janeiro, RJ, Brazil,* [§]*Faculdade de Ciências da Saúde, Universidade Federal do Amazonas, 69010-300, Manaus, AM, Brazil, and* [∥]*Departamento de Química Orgânica, Instituto de Química, Universidade Federal Fluminense, CEG, Campus do Valonguinho, 24210-141, Niterói, RJ, Brazil*

Received August 24, 2009

A class of drugs in use for treating type II diabetes mellitus (T2D), typified by the pseudotetrasaccharide acarbose, act by inhibiting the α-glucosidase activity present in pancreatic secretions and in the brush border of the small intestine. Herein, we report the synthesis of a series of 4-substituted 1,2,3-triazoles conjugated with sugars, including D-xylose, D-galactose, D-allose, and D-ribose. Compounds were screened for α-glucosidase inhibitory activity using yeast maltase (MAL12) as a model enzyme. Methyl-2,3-*O*-isopropylidene-*β*-D-ribofuranosides, such as the 4-(1-cyclohexenyl)-1,2,3-triazole derivative, were among the most active compounds, showing up to 25-fold higher inhibitory potency than the complex oligosaccharide acarbose. Docking studies on a MAL12 homology model disclosed a binding mode consistent with a transition-state-mimicking mechanism. Finally, the actual pharmacological potential of this triazole series was demonstrated by the reduction of postprandial blood glucose levels in normal rats. These compounds could represent new chemical scaffolds for developing novel drugs against T2D.

Introduction

A glycosidic bond is a covalent chemical bond that joins two simple sugars by means of an oxygen atom. Many polysaccharides are formed by monosaccharides joined by α or *β* glycosidic bonds. During the digestion process these bonds are hydrolyzed by specific glycosidases liberating the carbohydrate subunits as nutrients.[1]

In humans, four enzymes are responsible for the complete degradation of starch into glucose, which is then able to enter the bloodstream by a specific transport system.[2,3] First, salivary and pancreatic α-amylases (EC 3.2.1.1) cleave the internal α-1,4 bonds of starch into shorter linear and branched dextrin chains. The dextrins are then further hydrolyzed into glucose by two small-intestinal brush-border exohydrolases (maltase−glucoamylase, EC 3.2.1.20 and 3.2.1.3, and sucrase−isomaltase, EC 3.2.148 and 3.2.10).[4]

Human pancreatic α-amylase belongs to family 13 of the glycoside hydrolases (GH13[a]), which gathers a large variety of enzymes with varying substrate and product specificities as reflected by the 26 different EC numbers found in this family of enzymes: glycoside hydrolases (EC 3.2.1.X, the most abundant), glycoside transferases (EC 2.4.1.X), and even isomerases (EC 5.4.99.15 and EC 5.4.99.16).[5−7] Regardless of the low amino acid sequence similarity between the evolutionarily distant members of this family, some highly conserved residues are still present and structural studies have demonstrated that all GH13 members share similar folding.[8]

The α-glucosidase from *Saccharomyces cerevisiae* (baker's yeast), coded by the *MAL12* gene, is also a member of the GH13 family. It can hydrolyze nonreducing 1,4-linked α-D-glucose residues with release of α-D-glucose (EC 3.2.1.20) and retention of configuration at the anomeric carbon, characteristic of GH13 enzymes.[6,9] Because of its ready availability and ease of handling, baker's yeast α-glucosidase (MAL12) has been widely used in enzymatic assays to discover new α-glucosidase inhibitors with distinct biological activities.[10−16] In addition, MAL12 has been targeted in several structure-based drug design efforts where the lack of experimental information at the protein structure level has been mainly overcome by the use of theoretical models based on homology with the GH13 family members for which structural information is available.

Enzyme-catalyzed glycosidic bond cleavage of pyranosides is usually mediated by two catalytic carboxylic acid residues and typically proceeds via a positively charged oxocarbenium ion transition state.[17] The charge buildup is accompanied by planarization of the anomeric carbon and concomitant distortion of the pyranose ring out of its chair conformation. Many natural and synthetic glycosidase inhibitors mimic the charge buildup and/or the conformational distortion of the transition state.[11] Among them, nojirimycin (**1**) and deoxynojirimycin (**2**) are two classical glycosidase inhibitors isolated

*To whom correspondence should be addressed. Telephone: + 55 21 26292345. Fax: + 55 21 26292362. E-mail: cegvito@vm.uff.br.

[a]Abbreviations: GH13, family 13 of the glycoside hydrolases; GTase, 4-α-glucanotransferase; Ms, mesylate; Ts, tosylate; DMF, dimethylformamide; DMAP, dimethylaminopyridine; PDB, Protein Data Bank; LP, lipophilic potential; T2D, type II diabetes mellitus; HRMS, high-resolution mass spectrometry.

 Published on Web 02/19/2010

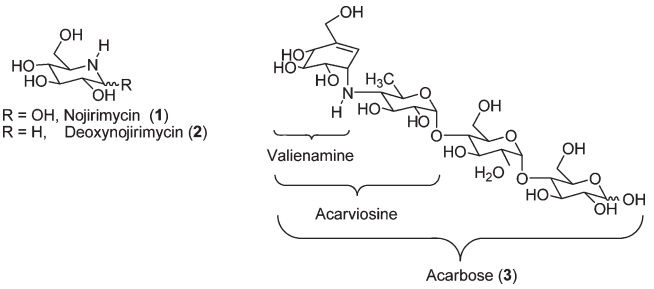

Figure 1. Natural glycosidase inhibitors.

from the cultured broth of a *Streptomyces* sp., acting on the early stages of glycoprotein processing.

The search for α-glucosidase inhibitors led to the discovery of acarbose (**3**), a pseudotetrasaccharide isolated from the *Actinoplanes* strain SE 50 as a potent sucrase inhibitor. Acarbose consists of a polyhydroxylated aminocyclohexene derivative (valienamine) linked via its nitrogen atom to a 6-deoxyglucose, which is itself α-1,4-linked to a maltose moiety (Figure 1).[18]This compound inhibits porcine intestinal sucrase with an IC_{50} of 0.5 μM.[19] After many clinical investigations it was introduced on the market in 1990 for the treatment of type 2 diabetes mellitus,[2] since inhibition of pancreatic α-amylase and intestinal α-glucosidases has demonstrated great value in the control of postprandial blood glucose levels by slowing the starch digestion rate.[20−24] The strong inhibition of human amylases by acarbose (micromolar K_i) is attributed both to the partial planarity of the valienamine ring and to the presence of strong electrostatic interactions between the carboxyl groups at the active site and the protonated nitrogen atom of the inhibitor.[2]

The importance of triazolic compounds in medicinal chemistry is undeniable. Particularly, 1,2,3-triazoles have gained increased attention in the drug-discovery field since the introduction of the "click" chemistry concept by Sharpless.[25,26] These types of compounds can actively participate in hydrogen bonding and dipole−dipole interactions because of their strong dipole moments and are extremely stable to hydrolysis and oxidative/reductive conditions. Moreover, contrary to other azaheterocycles, the 1,2,3-triazole ring is not protonated at physiological pH because of its poor basicity. Hence, it has been proposed that the nonprotonated sp^2-hybridized nitrogen atoms of 1,2,3-triazoles may better mimic the partial positive charge at the anomeric carbon in the transition state of the glucosidase catalyzed reaction than the corresponding basic nitrogen atoms of iminosugars.[27] By this reasoning, sp^2-azaheterocyclic glycomimetics may actually behave as more specific glucosidase inhibitors.

Rossi and Basu[28] have reported the synthesis of 1-glycosyl-4-phenyltriazoles linked to the anomeric carbon atom of the sugar unit, with one galactosyl derivative showing K_i for *Escherichia coli* β-galactosidase of about 300 μM. In another work, Périon et al.[29] reported the synthesis of 6-deoxyglucosyl-triazoles (linked via C4 of the sugar unit) with a 2-fold higher inhibitory activity against yeast α-glucosidase (K_i = 73 μM) than acarbose.

In this paper, we report the synthesis of novel 1*H*-1,2,3-triazoles attached to carbohydrates, their in vitro evaluation as α-glucosidases inhibitors and demonstrate their hypoglycemic activity in normal rats for two of the most potent inhibitors. A molecular modeling study was also undertaken to provide a structural rationale for the observed inhibitory potencies over yeast maltase.

Chemistry

The diversity of chemical structures of the 1,2,3-triazole family and their useful biological activities made these compounds attractive targets in synthetic organic chemistry. The potential of this heterocycle led us to develop a synthetic route for preparing glycoconjugated triazoles and examine their activity. The methodology used for obtaining the triazoles **4a**−**n**, **5a**, **6a**, and **7a**−**c** was based on the Huisgen 1,3-dipolar cycloaddition reaction.[30] In order to obtain only the 1,4 regioisomer we used the reaction conditions known as "click chemistry", which uses Cu(I) as a catalyst. In addition to increasing the reaction rate, the use of the copper catalyst provides full control over reaction regioselectivity leading only to the 1,4 regioisomer.[31] As observed by Sharpless, speed and reaction yields are much higher than with the traditional method, with yields above 80% and 100% of regioselectivity. Different terminal alkynes (**8a**−**n**) were used as substrates for the reactions with azido derivatives of ribose (**9**), xylose (**10**), galactose (**11**), and allose (**12**). Following preparation of the carbohydrate acetonides, a better leaving group at carbon C5, the target of the subsequent reactions, was obtained by tosylation or mesylation. Then the azido carbohydrates were prepared by a nucleophilic substitution reaction with sodium azide. According to Scheme 1, to obtain the 1,2,3-triazoles, a solution of an azido carbohydrate (D-ribose, D-xylose, D-allose, or D-galactose), a terminal alkyne, and copper sulfate pentahydrate (5 mol %) was treated with the slow addition of sodium ascorbate (15 mol %).[32] The reaction mixture was stirred for 4−6 h depending on the initial substrate. All the triazoles were obtained with good yields and fully characterized by ^{1}H NMR, ^{13}C NMR, IR (infrared) spectroscopy, HRMS (high-resolution mass spectra), and elemental analysis.

α-Glucosidase Inhibition

All compounds were initially screened for α-glucosidase inhibition at 500 μM, and the results are shown in Table 1. All compounds inhibited yeast maltase to some degree, and most of them presented an inhibitory profile higher than acarbose. Notably, most of the β-D-ribosyl derivatives **4a**, **4b**, **4d**, **4e**, **4f**, and **4g** as well as the α-D-galactosyl derivative **5a** and the α-D-xylosyl derivative **7a** produced the highest inhibitory values at 500 μM (Table 1).

Next, the determination of the IC_{50} for some of the most active β-D-ribosyl derivatives revealed that all of the tested triazoles presented higher inhibitory potencies against α-glucosidase than acarbose, with values ranging from 4 to 25 μM (Table 2). Compounds **4b**, **4e**, and **4g**, carrying, respectively, the 1-cyclohexenyl, phenoxymethyl, and 1-cyclohexanol moieties at C4 of the triazole ring, were the most active.

Molecular Modeling

Structure and Validation of Modeled Yeast Maltase (MAL12). The α-glucosidase MAL12 model consists of a single polypeptide chain of 576 residues, similar to *Bacillus cereus* and *Geobacillus sp.* glucosidases, which are also members of the GH13 family. Figure 2 shows the structural alignment between MAL12 and the templates used to construct the homology model.

As depicted in Figure 3, the model is composed of three domains: the N-terminal (residues 1−104 and 176−500), the subdomain (residues 105−175), and the C-terminal domain

Scheme 1. Synthesis of 1*H*-1,2,3-Triazole Derivatives of Carbohydrates

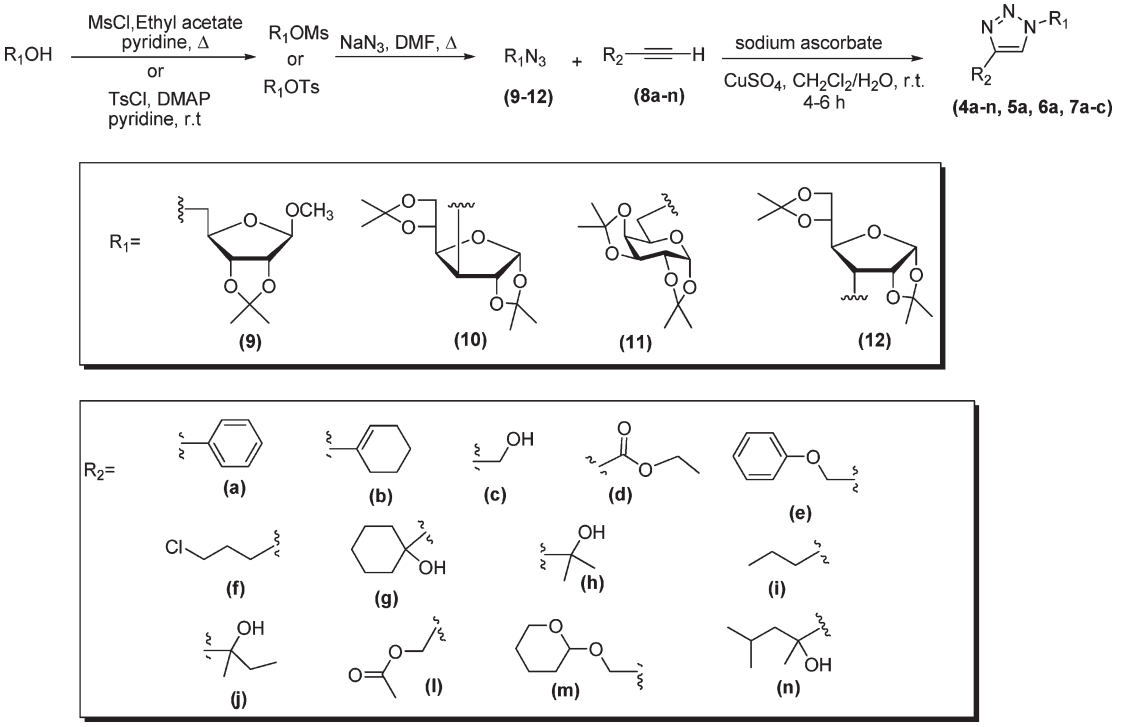

Table 1. Inhibitory Activities of 1*H*-1,2,3-Triazole Derivatives at 500 μM over Yeast α-Glucosidase[a]

compd	inhibition (%)
acarbose	48.1 ± 1.9
4a	94.4 ± 7.5
4b	98.1 ± 0.3
4c	46.5 ± 16.4
4d	98.0 ± 1.3
4e	98.4 ± 3.7
4f	99.5 ± 0.1
4g	98.5 ± 0.3
4h	60.2 ± 13.1
4i	44.9 ± 3.1
4j	41.1 ± 18
4l	nd
4m	79.5 ± 2.5
4n	nd
5a	99.4 ± 0.4
6a	73.1 ± 1.4
7a	87.9 ± 13.5
7b	33.3 ± 46.1
7c	68.8 ± 20

[a] nd: not determined.

Table 2. IC_{50} Values of β-D-Ribosyltriazoles **4a**, **4b**, **4d**, **4e**, **4g**, **4m**, and Acarbose over Yeast Maltase

compd	IC_{50} (μmol/L)
acarbose	108.8 ± 12.3
4a	14.9 ± 4.2
4b	3.8 ± 0.5
4d	15.1 ± 0.9
4e	5.7 ± 0.3
4g	5.2 ± 0.9
4m	24.7 ± 11.8

(residues 500−576). The catalytic residues (Asp206, Glu268, and Asp341) are found in the N-terminal domain, as with all glucosidases of the GH13 family.[11] The substrate binding cleft is aligned between the N-terminal domain and the subdomain. No disulfide bond was found in the structure.

The stereochemical quality of the model was evaluated using the ProCheck program[33] with 99% of the residues found with allowed backbone conformations, according to the Ramachandran plot. Only four residues (0.8%) lay in generously allowed regions, and just one residue (0.2%) had a disallowed conformation (Phe302). Other stereochemical parameters for the MAL12 model were inside the expected values. The compatibility between the amino acid sequence and the environment of the amino acid side chains in the model was further checked with the Verify-3D program, which uses a 3D score for each residue type in each environmental class to pinpoint residues with unusually low scores that may indicate an incorrect structure.[34] In the MAL12 model, around 86% of the residues had an averaged 3D−1D score of >0.2, indicating a possible correct folding of the protein.

Identification of the Substrate Binding Subsites on MAL12. On the basis of the fact that the catalytic residues (Asp206, Glu268, and Asp341 in MAL12) and the residues important for substrate binding (Tyr63, His103, and His340 in MAL12) are highly conserved in the GH13 family,[11,35] we used the conformation of modified acarbose in the complex with *T. maritima* 4-α-glucanotransferase (PDB code 1LWJ)[9] to define the binding site for docking acarbose to MAL12. The resulting bound conformation of acarbose in MAL12 was consistent with the binding mode of this pseudosaccharide or its analogues to other GH13 glucosidases. The analysis of this modeled complex enabled the identification of four subsites involved in substrate binding to MAL12: −1, +1, +2, and +3 (following the nomenclature of Davies et al.[36]).

The −1 and +1 subsites are involved in the recognition of the acarviosine unit in acarbose. In addition to the catalytic residues, Asp60, Tyr63, His103, Phe169, Gln173, and Arg431

```
MAL12   1   TEPKWWKEATIYQIYPASFKDSNNDGWGDLKGITSKLQYIKDLGVDAIWV  50
1UOK    1   MEKQWWKESVVYQIYPRSFMDSNGDGIGDLRGIISKLDYLKELGIDVIWL  50
2ZE0    1   -KKTWWKEGVAYQIYPRSFMDANGDGIGDLRGIIEKLDYLVELGVDIVWI  49

MAL12  51   CPFYDSPQQDMGYDISNYEKVWPTYGTNEDCFELIDKTHKLGMKFITDLV 100
1UOK   51   SPVYESPNDDNGYDISDYCKIMNEFGTMEDWDELLHEMHERNMKLMMDLV 100
2ZE0   50   CPIYRSPNADNGYDISDYYAIMDEFGTMDDFDELLAQAHRRGLKVILDLV  99

MAL12 101   INHCSTEHEWFKESRSSKTNPKRDWFFWRPPKGYDAEGKPIPPNNWKSFF 150
1UOK  101   VNHTSDEHNWFIESRKSKDNKYRDYYIWRPGK----EGKE--PNNWGAAF 144
2ZE0  100   INHTSDEHPWFIESRSSRDNPKRDWYIWRDGK----DGRE--PNNWESIF 143

MAL12 151   GGSAWTFDETTNEFYLRLFASRQVDLNWENEDCRRAIFESAVGFWLDHGV 200
1UOK  145   SGSAWQYDEMTDEYYLHLFSKKQPDLNWDNEKVRQDVYE-MMKFWLEKGI 193
2ZE0  144   GGSAWQYDERTGQYYLHIFDVKQPDLNWENSEVRQALYE-MVNWWLDKGI 192

MAL12 201   DGFRIDTAGLYSKRPGLPDSPIFDKTSKLQHPNWGSHNGPRIHEYHQELH 250
1UOK  194   DGFRMDVINFISKEEGLPTVETEEEG--YVSGHKHFMNGPNIHKYLHEMN 241
2ZE0  193   DGFRIDAISHIKKKPGLPDLP-----LKYVPSFAGHMNQPGIMEYLRELK 237

MAL12 251   RFMKNRVKDGREIMTVGEVAHGS--DNALYTSAARYEVSEVFSFTHVEV- 297
1UOK  241   ----EEVLSHYDIMTVGEMPGVTTEEAKLYTGEERKELQMVFQFEHMDL- 286
2ZE0  237   ----EQTFARYDIMTVGEANGVTVDEAEQWVGEENGVFNMIFQFEHLGLW 283

MAL12 298   GTSPFFRYNIVPFTLKQWKEAIASNFLFINGTDSWATTYIENHDQARSIT 347
1UOK  287   DSGEGGKWDVKPCSLLTLKENLTKWQKALEHT-GWNSLYWNNHDQPRVVS 335
2ZE0  284   ERRA--SIDVR-----RLKRTLTKWQKGLENR-GWNALFLENHDLPRSVS 325

MAL12 348   RFADDSPKYRKISGKLLTLLECSLTGTLYVYQGQEIGQINFKEWPIEKYE 397
1UOK  336   RFGNDG-MYRIESAKMLATVLHMMKGTPYIYQGEEIGMTNVRFESIDEYR 384
2ZE0  326   TWGNDR-DYWAESAKALGALYFFMQGTPFIYQGQEIGMTNVRFDDIRDYR 374

MAL12 398   DVDVKNNYEIIKKSFGKNSKEMKDFFKGIALLSRDHSRTPMPWTKDKPNA 447
1UOK  385   DIETLN---MYKEKVMERGEDIEKVMQSIYIKGRDNARTPMQWD-DQNHA 430
2ZE0  375   DVSALR--------------------IIWKTGRDNSRTPMQWS-GASNA 402

MAL12 448   GFTGPDVKPWFLLNESFEQGINVEQESRDDDSVLNFWKRALQARKKYKEL 497
1UOK  431   GFTTGE--PWITVNPNYKE-INVKQAIQNKDSIFYYKKLIELRKN-NEI 476
2ZE0  403   GFTTGT--PWIKVNENYRT-INVEAERRDPNSVWSFYRQMIQLRKA-NEL 448

MAL12 498   MIYGYDFQFIDLDSDQIFSFTKEYEDKTLFAALNFSGEEIEFSLPREG-- 545
1UOK  477   VVYG-SYDLILENNPSIFAYVRTYGVEKLLVIANFTAEECIFELPEDISY 525
2ZE0  449   FVYG-TYDLLLENHPSIYAYTRTLGRDRALVVVNLSDRPSLYRY-DGFRL 496

MAL12 546   ASLSFILGNYD---DTDVSSRVLKPWEGRIYLVK 576
1UOK  526   SEVELLIHNYDVE-NGPIENITLRPYEAMVFKLK 558
2ZE0  497   QSSDLALSNYPVRPHKNATRFKLKPYEARVYIWK 530
```

Figure 2. Sequence alignment of MAL12, oligo-1,6-glucosidase from *Bacillus cereus* (PDB code 1UOK), and GH13 α-glucosidase from *Geobacillus sp* (GSJ, PDB code 2ZE0). The alignment was shaded according to the Blosum62 matrix at the 100% conservation level.

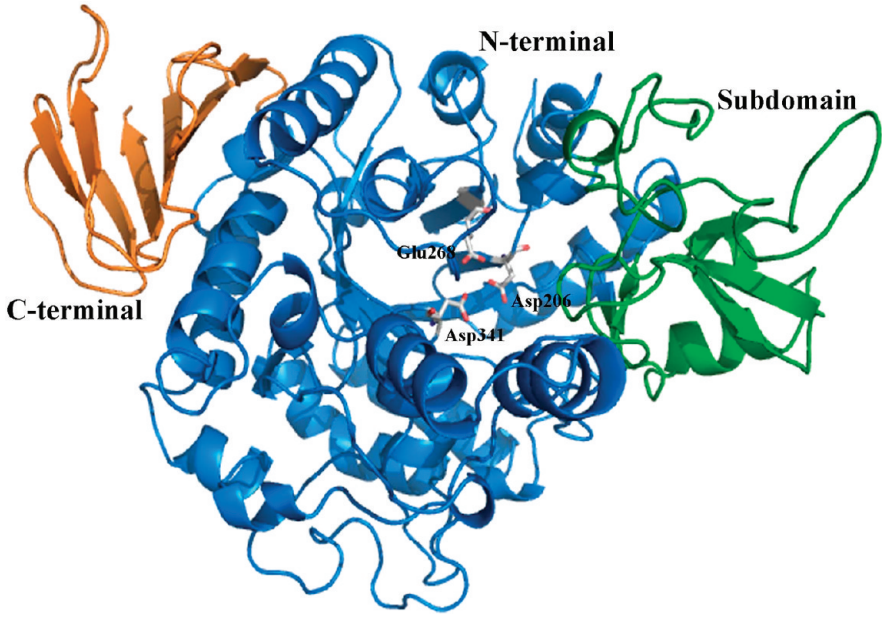

Figure 3. Graphic representation of the homology modeling structure of MAL12. The N-terminal, subterminal, and C-terminal domains are shown in blue, green, and orange, respectively. The catalytic residues are highlighted.

surround the valienamine moiety while residues Thr207 and His340 are closer to the 6-deoxyglucose subunit. The +2 subsite is formed by residues Phe149, His231, Asn233, and Ala270, while the +3 subsite is formed by residues His271, Glu296, Thr299, and Phe303. In contradiction to the observations of Tomich et al.,[38] we found that the MAL12 structure could not accommodate a −2 subsite (occupied by the 6-deoxyglucose moiety in the nonreducing terminal of modified acarbose modeled by these authors). In our model of MAL12, the residues Asp60, Tyr63, Phe150, Asn173, and Arg431 form the bottom of a substrate binding cleft that effectively blocks the binding of an oligosaccharide extending beyond the −1 residue. This observation is consistent with the known specificity of MAL12, which removes an α-linked glucose unit from the nonreducing end of a carbohydrate chain.

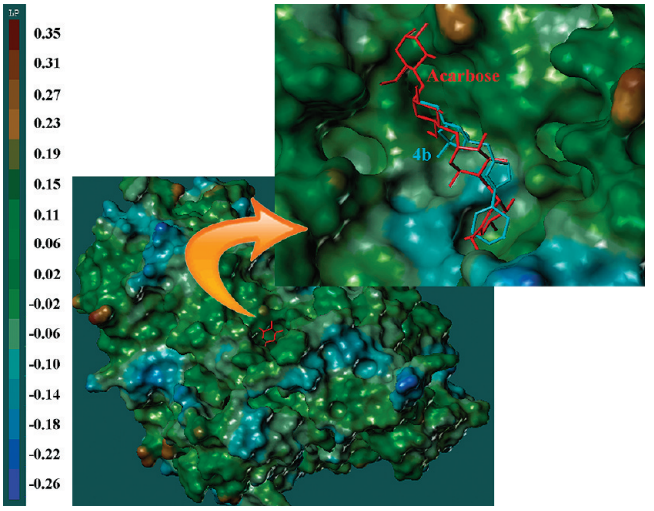

Figure 4. Superposition of the docked conformations of acarbose (red) and compound **4b** (cyan) in the MAL12 binding site. The protein surface was colored by the lipophilic potential (LP) calculated using the MOLCAD module of the Sybyl molecular modeling package (Tripos Associates, St. Louis, MO). The color ramp ranges from brown (most lipophilic) to blue (most hydrophilic). In the detail (inset), the molecular surface regions corresponding to the protein segments Gln58-Asp64, Glu397-Ser416, Lys147-Ser153, Tyr211-His231, Arg167-Arg172, Ser300-Asn306 were omitted to render a clearer view of the floor of the substrate binding cleft in MAL12.

Molecular Docking of 1,2,3-Glucotriazoles. All of the compounds used in the docking study consist of a triazole moiety coupled via a β-glycosidic linkage to D-ribose monoacetonide, and the chemical differences lie in their distinct R_2 substituents (see Table 2). The MAL12−ligand complexes were generated by docking the triazoles into the enzyme active site, assuming a competitive inhibition mechanism, similar to acarbose[2] (Figure 4).

A visual inspection of the highest-scoring docking conformations for the triazole compounds revealed a recurrent configuration where the R_2 substituent was located at the −1 subsite, corresponding to the position of the valienamine moiety in acarbose. Moreover, in this position the triazole ring is found occupying the +1 subsite, where it makes a hydrogen bond with Glu268, while the D-ribose monoacetonide moiety binds to the region encompassing the +2 subsite and part of the +3 subsite (Figure 4). This binding mode is consistent with a transition-state-mimicking mechanism, as proposed for other triazoles,[32] and acknowledges the importance of the interaction with Glu268 as a significant feature in the inhibition of yeast α-glucosidase and other GH13 enzymes, as was previously proposed.[15] Another point considered to identify the most likely binding mode for the ligands was the placement of the R_2 group in the −1 subsite, since compounds with bulk R_2 substituents (except for **4a**) were among the most potent of the series under study, which indicates that this molecular region is likely to be completely buried inside the enzyme.

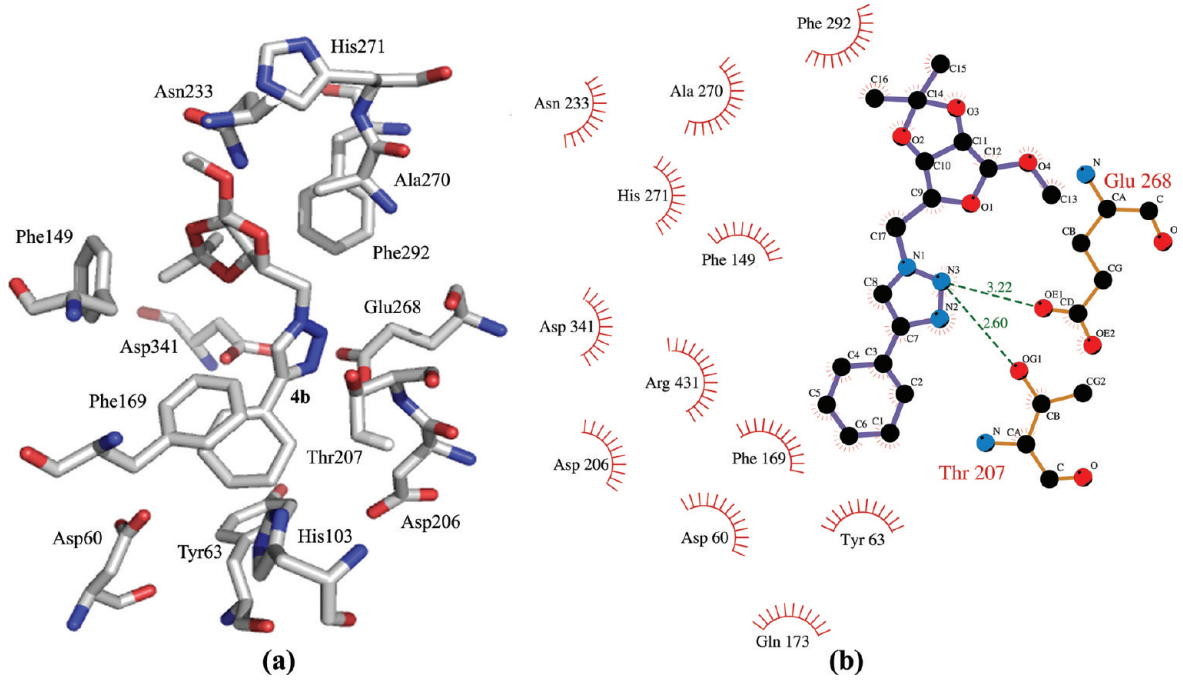

Figure 5. Binding mode of compound **4b** in the MAL12 active site: (a) important residues for **4b** binding in the MAL12 active site, according to visual inspection, considering the amino acid residues in a radius of 6 Å around the ligand; (b) Ligplot[40] cartoon illustrating compound **4b** binding to MAL12.

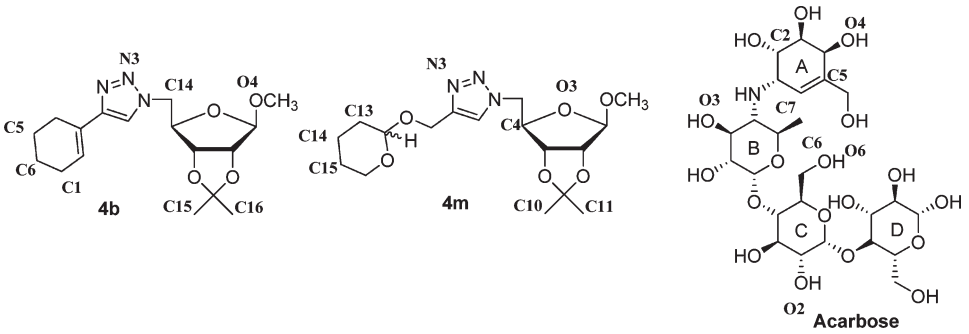

Ligand		Residue		Distance (Å²)[a]	Type of Contact[b]	Surface (Å²)[c]
Name	Atom	Name	Atom			
4b	C6	Tyr63	CB	3.3	Ph	25.6
	C5	His103	CE1	3.3	Ph	23.8
	C15	Phe149	CZ	3.3	Ph	27.8
	C1	Phe169	CD1	3.7	Ph	14.4
	N3	Thr207	OG1	2.6	HB	39.8
	N3	Glu268	OE1	3.2	HB	11.5
	C14	Ala270	CB	3.9	Ph	9.2
	O4	Asn233	ND2	3.3	HB	9.2
4mR	C15	Tyr63	CB	3.4	Ph	17.0
	C14	His103	CE1	3.4	Ph	20.6
	C10	Phe149	CD1	3.8	Ph	17.7
	C14	Phe169	CZ	3.7	Ph	13.2
	C13	Thr207	CG2	3.5	Ph	20.6
	C10	Ala270	CB	3.6	Ph	13.9
	C11	His271	CD2	4.2	Ph	3.8
4mS	C15	Tyr63	CE2	3.3	Ph	19.3
	C10	Phe149	CE1	3.5	Ph	23.3
	C13	Phe169	CE1	2.4	Ph	34.8
	N3	Glu268	OE1	2.7	HB	2.2
	C11	Ala270	CB	4.9	Ph	4.0
	C11	His271	CD2	4.6	Ph	3.4
	O3	Arg304	NH2	2.9	HB	10.0
Acarbose	C5A	Tyr63	CD2	4.4	Ph	0.9
	C7A	His103	CE1	4.8	Ph	0.2
	C6B	Phe149	CD2	3.6	Ph	24.7
	C6B	Phe169	CD1	4.0	Ph	4.5
	O3B	Asn233	ND2	2.7	HB	24.4
	O2C	His271	NE2	2.9	HB	11.1
	O6C	Arg304	NE	3.4	HB	25.5
	O2A	His340	NE2	3.0	HB	9.7
	O4A	Arg431	NH1	2.9	HB	20.6

[a] Nearest distance (Å) between atoms of the ligand and the residue.
[b] Type of Contacts: (HB) hydrogen bond; (Ph) hydrophobic-hydrophobic; (Ar) aromatic.
[c] Contact surface area (Å²) between the ligand and the residue.

Figure 6. Comparison of the atomic contacts established between MAL12 and the ligands **4b**, **4m** stereoisomers *R* and *S* (**4mR** and **4mS**), and acarbose.

Figure 5 depicts the binding mode of compound **4b**, one of the most potent compounds of the series under study. It is noted that the important residues for substrate binding and/or catalysis[39] are present in the binding site (Tyr63, His103, Asp206, Glu268, His340, and Asp341). Additionally, a strong hydrogen bond is established between the nitrogen atom of the triazole moiety and the Thr207 (O−N distance of 3.0 Å) and Glu268 (O−N distance of 3.2 Å) residues.

Figure 6 provides a detailed comparison of the atomic contacts established between MAL12 and compounds **4b** and **4m** (stereoisomers *R* and *S* of the latter) to delineate features in the binding modes of the most and the least potent triazole derivatives acting as α-glucosidase inhibitors, respectively. Acarbose was also included as a reference drug.

The distorted half-chair conformation of the cyclohexenyl ring is an important part of the interaction of compound **4b** with MAL12. This substituent is stabilized by several hydrophobic contacts with Tyr63, His103, and Phe169, being actually sandwiched by Tyr63 and Phe169, similar to the valienamine moiety of modified acarbose in the complex with *T. maritima* 4-α-glucanotransferase.[37] The isopropylidene group of **4b** also forms hydrophobic interactions with Phe149, Ala270, and His271.

Triazole **4d** showed almost 3-fold lower potency than **4b** (IC_{50} = 15.1 ± 0.9 μol/L, Table 2) and is the only compound presenting an acyclic and significantly more polar R_2 substituent. The analysis of the **4d**−MAL12 complex shows that the triazole moiety of compound **4d** makes hydrogen bonds with Thr207 (O−N distance of 3.9 Å) and Glu268

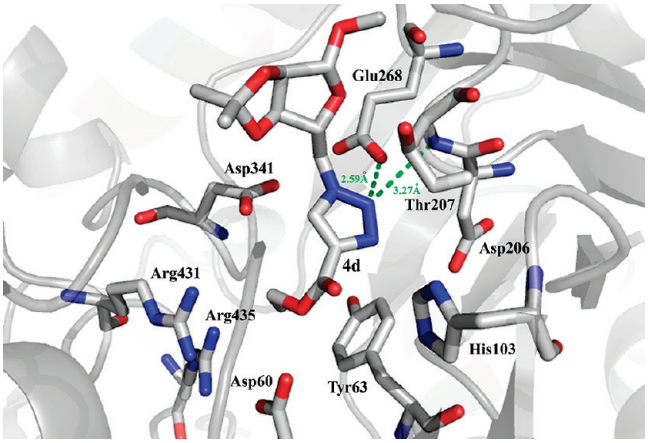

Figure 7. Docked conformation of compound **4d** on the MAL12 model (gray). The slab shown depicts residues important to inhibitor binding. The triazole moiety makes hydrogen bonds with Thr207 and Glu268, but the ligand does not produce hydrophobic contacts with Tyr63 and His103.

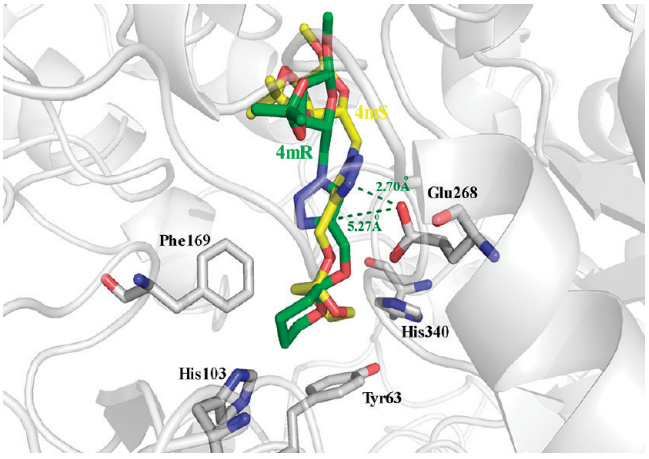

Figure 8. Superposition of docked conformations of **4mS** (CPK colored with carbon atoms in yellow) and **4mR** (CPK colored with carbon atoms in green) on the MAL12 model. The figure was drawn in slab mode to show residues important to inhibitor binding. As can be seen, molecule **4mR** does not make a hydrogen bond with Glu268.

(O−N distance of 2.6 and 3.6 Å for OE2 and OE1 atoms, respectively). However, the ligand does not seem to produce hydrophobic contacts with Tyr63, His103, and Phe169, probably because of the polar nature of the shorter R_2 substituent (Figure 7). Moreover, the amide substituent of **4d** shows a destabilizing contact with the Tyr63 side chain.

Compound **4m** was the least potent of the series, although it has a bulky R_2 substituent. The key to understanding this apparent inconsistency is that this compound was tested as a racemic mixture. Consequently, the docking procedure was performed with both enantiomers (*R* and *S*) aiming to recognize how they individually contribute to the inhibition of the enzyme.

The *S* configuration of compound **4m** (**4mS**) interacts through hydrogen bonds with Arg304 (**4mS**, O1−N distance of 2.9 Å), Thr207 (triazole moiety, O−N distance of 3.2 Å), and Glu268 (**4mS**, N2−O distance of 3.2 Å) (Figure 6). Similar to the cyclohexyl moiety in compound **4b**, the tetrahydropyranyl substituent of compound **4mS** also forms hydrophobic contacts with residues Tyr63, His103, Phe169, and His340, and the isopropylidene group interacts with Phe149, Ala270, and His271 (Figure 6).

With the R configuration of compound **4m** (**4mR**), the oxymethylene moiety displaces the triazole group in order to maintain the favorable hydrophobic interactions of the tetrahydropyranyl group. However, the molecule loses the hydrogen bond with Glu268 (Figure 8). The absence of such interaction for the *R* enantiomer may be a reason why **4m** is the least potent compound of the series, since it is described as an important interaction to the α-glucosidase inhibition.[15]

One limiting factor in the docking approach used here is the lack of a solvation term in the scoring function, since solvation effects have been evoked previously to explain poor structure−activity relationships with non-carbohydrate glucosidase inhibitors.[41] In fact, we could not find any reasonable correlation between the docking energies and inhibitory potencies of the examined compounds.

On another issue, compounds **4a**, **4b**, **4d**, **4e**, **4g**, and **4m** showed higher inhibitory potencies than acarbose, and the docking studies presented here were unable to offer an

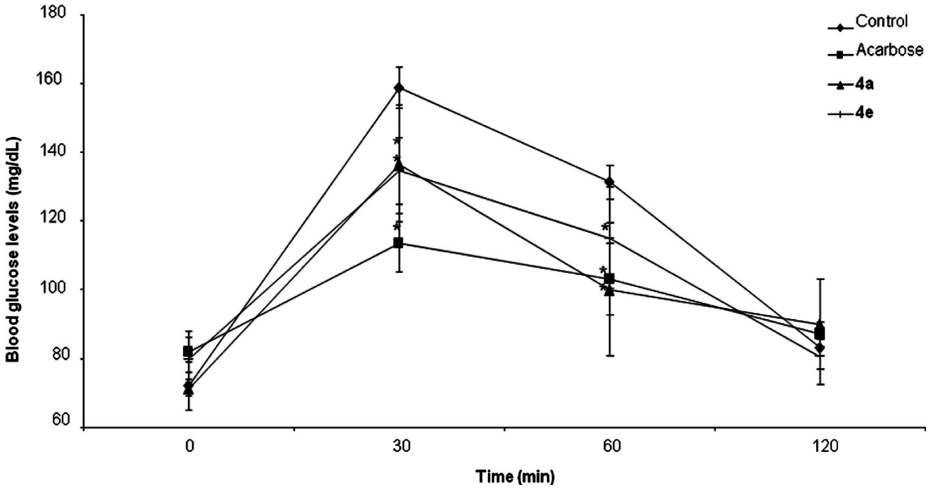

Figure 9. Effect of triazoles and acarbose after a single oral administration of 3 g/kg maltose in normal rats. Five hundred milliliters of 50 mg/kg triazoles or acarbose was dosed. After 5 min, 1 mL of a 3 g/kg maltose solution was administered to each rat. Control group was administered with the same volume of maltose solution without inhibitor. At 0, 30, 60, and 120 min, 20 μL blood samples were collected and immediately subjected to blood glucose level assays by a disposable glucose sensor. Data are the mean (mg/dL of plasma) ± SD. Significant differences between sample and control groups were examined with Dunnett's *t*-test ($n = 5$, (∗) $P < 0.05$).

unambiguous structural explanation for this, as the acarbose−MAL12 complex shows extensive favorable contacts between this pseudotetrasaccharide and the enzyme (Figure 6). One possible origin for this difficulty is in the entropic contribution to binding, which is usually not taken into account when a docking study is performed. Indeed, acarbose is the most flexible of the α-glucosidase ligands examined in this work, having six free-rotating bonds connecting its four rings (three more than compound **4b**). Rigid ligands are likely to face less entropic penalties upon binding than a more flexible one and thus should have a more favorable binding energy.[42] Given the comparison with the bound conformations of the triazoles (Figure 4), it is likely that the interactions made by the fourth ring of acarbose cannot compensate for the entropic cost of correctly positioning this additional ring in the MAL12 binding cleft. Consistent with this view, the pseudotrisaccharide, acarviosine−glucose, has been shown to be a 400-fold more potent inhibitor of yeast α-glucosidase than acarbose.[43]

Hypoglycemic Effect in Normal Rats

In order to investigate the pharmacological potential of the most active α-glucosidase inhibitors in the triazole series as leads for developing new drugs for T2D, we assayed compounds **4a** and **4e** for hypoglycemic activity in normal rats. The selected triazoles were resynthesized on a 2 g reaction scale, and no significant changes in the reaction yields were noted for this increased scale. Upon oral administration at a 50 mg/kg dose, compounds **4a** and **4e** were able to significantly reduce glucose uptake by normal rats fed with maltose (Figure 9). This hypoglycemic effect was more evident 30 and 60 min after maltose ingestion, when blood glucose levels were peaking, similar to the effect displayed by the reference drug acarbose. The latter clearly performed better than compound **4e** in reducing glucose levels in blood samples collected at 30 and 60 min but was undistinguishable from compound **4a** for the 60 min sample.

Conclusions

We have described the synthesis of several 1*H*-1,2,3-triazole derivatives of carbohydrates and have demonstrated their action as α-glucosidase inhibitors. The α-glucosidase inhibition screening showed that all compounds were active at 500 μM, although the triazoles conjugated with D-ribose (**4a**−**n**) were in general more effective than the other triazoles containing D-xylose, D-galactose, and D-allose as the carbohydrate portion (**5a**, **6a**, **7a**−**c**). The 1-*O*-methyl-2,3-*O*-isopropylidene-β-D-ribofuranose derivatives were conjugated through the C5 atom of the sugar and the N1 atom of the 1*H*-1,2,3-triazole ring. Some of these compounds, e.g., **4b**, **4e**, and **4g**, showed 20-fold higher potency in yeast maltase inhibition than acarbose, as measured by the ratios of their IC_{50} values. This observation was quite surprising considering the specificity of this enzyme for substrates containing at least one and up to four glucose residues linked by α-1,4 bonds. Moreover, compounds **4a** and **4e**, reduced postprandial glucose levels when administered orally to normal rats, highlighting the pharmacological potential of this synthetic series. While assuming a reversible competitive inhibition modality for these compounds, our molecular modeling study supported a binding mode compatible with a transition-state mimicking mechanism, where the most potent inhibitors have the N3 atom in the triazole ring bound to one of the catalytic carboxylates, Glu268, and the R_2 substituent engaging important hydrophobic contacts with residues Tyr63, His103, and Phe169 at the −1 subsite. The computational study also predicted that the *R* enantiomer within the racemic compound **4m** may have little or no activity because of the lack of the crucial interaction with Glu268 in the active site. Although successful in offering a possible structural rationale for the inhibition mechanism of these triazoles, the molecular modeling study could not correlate interaction energies calculated from the docked conformations of the ligands with experimental binding affinities. This difficulty may have arisen from the oversimplistic physical model used in the docking program, where neither entropic contributions nor solvation terms were included in the binding-energy computation. Moreover, it is possible that some of these inhibitors may not work as purely competitive inhibitors, presenting mixed (noncompetitive) behavior instead. It is noteworthy that the compounds were tested with all or most of the sugar hydroxyl groups protected by an isopropylidene moiety. The presence of these protecting groups may have a huge effect on the inhibitory activities of these compounds because of the increased molecular volume and loss of donor hydrogen-bonding groups. Work is underway in our group to clarify all of these issues. Indeed, the high efficiency of the proposed synthesis, in combination with the plethora of readily available azide and acetylene reagents, makes the approach particularly well suited for combinatorial library schemes, which should facilitate hypothesis testing and optimization of inhibitor potencies.

Experimental Section

Chemistry. General Remarks. Reagents were used as purchased without further purification. Reagents were purchased from Aldrich or Acros Chemical Co. Dichloromethane and DMF were distilled from calcium hydride. Pyridine was distilled from potassium hydroxide. Acetone was distilled from phosphorus pentoxide and methanol from iodine and magnesium. Column chromatography was performed with silica gel 60 (Merck 70−230 mesh). Analytical thin-layer chromatography was performed with silica gel plates (Merck, TLC silica gel 60 F254), and the plots were visualized under UV light or developed by immersion in an ethanolic solution of vanillin. Yields refer to chromatographically and spectroscopically homogeneous materials. Melting points were obtained on a Fischer−Johns apparatus and are uncorrected. Infrared spectra data were recorded from KBr pellets on a Perkin-Elmer model 1420 FT-IR spectrophotometer calibrated relative to the 1601.8 cm^{-1} absorbance of polystyrene. The optical rotations ($[\alpha]_{20}^{D}$) were measured with a Perkin-Elmer 243B polarimeter using 10 cm cells and a wavelength of 589 nm. NMR spectra were recorded on a Varian Unity Plus VXR (300 MHz) system in $CDCl_3$ solutions using tetramethylsilane as the internal reference standard (0.0 ppm). Coupling constants (*J*) are reported in hertz and refer to apparent peak multiplicities. HRMS were recorded on a MICROMASS Q-TOF MICRO mass spectrometer using ESI-TOF (electrospray ionization time-of-flight). Elemental analysis was used to ascertained purity of ≥95% for all compounds for which biological data were determined.

General Method for the Preparation of 1*H*-1,2,3-Triazoles Derivatives 4a−n, 5a, 6a, and 7a−c. To a solution containing 0.70 mmol of the appropriate alkyne, 0.83 mmol of azidocarbohydrates in dichloromethane (0.7 mL), and water (0.7 mL) were added $CuSO_4 \cdot 5H_2O$ (9.3 mg, 0.04 mmol) and sodium ascorbate (22 mg, 0.11 mmol). The resulting suspension was stirred at room temperature for 4−6 h. After this time, the mixture was diluted with 5 mL of dichloromethane and 5 mL of water. The organic phases were separated, dried with sodium sulfate, and concentrated at reduced pressure, furnishing the 1,2,3-triazoles

derivatives, which were analyzed by ^{1}H and ^{13}C NMR spectroscopy and infrared.

1-*O*-Methyl-2,3-*O*-isopropylidene-5-(4-phenyl-1*H*-1,2,3-triazol-1-yl)-β-D-ribofuranose (4a). Compound **4a** was obtained as a white powder in 98% yield. Mp 130−133 °C. $[\alpha]_{20}^{D}$ −46 (*c* 1.0, $CHCl_3$). IR (film, $CHCl_3$) ν (cm^{-1}): 3075 and 1612. ^{1}H NMR ($CDCl_3$, 300 MHz) δ 1.31 (s, 3H, CH_3), 1.47 (s, 3H, CH_3), 3.41 (s, 3H, OCH_3), 4.43 (d, 1H, J = 5.8 Hz, H-3′), 4.62−4.70 (m, 3H, H-5′ and H-4′), 4.79 (d, 1H, J = 5.8 Hz, H-2′), 5.04 (s, 1H, H-1′), 7.31−7.45 (m, 3H, ArH), 7.82−7.87 (m, 3H, ArH and H-5). ^{13}C NMR ($CDCl_3$, 75 MHz) δ 24.7 (CH_3), 26.2 (CH_3), 55.4 (OCH_3), 53.0 (C-5′), 81.6 (C-2′), 84.8 (C-3′), 85.0 (C-4′), 109.9 (C-1′), 112.7 (C-6′), 119.7 (C-5), 125.5 (C-Ar-2a or 3a or 4a), 128.0 (C-Ar-2a or 3a or 4a), 128.6 (C-Ar-2a or 3a or 4a), 130.3 (C-Ar-1a), 147.8 (C-4). HRMS (EI) calcd for $C_{17}H_{21}N_3O_4$: 331.1532. Found: 332.3803 $(M + H)^+$. Anal. Calcd for $C_{17}H_{21}N_3O_4$: C, 61.62; H, 6.39; N, 12.68. Found: C, 61.63; H, 6.40; N, 12.70.

1-*O*-Methyl-2,3-*O*-isopropylidene-5-(4-cyclohexene-1*H*-1,2,3-triazol-1-yl)-β-D-ribofuranose (4b). Compound **4b** was obtained as a light-yellowish powder in 95% yield. Mp 105−108 °C. $[\alpha]_{20}^{D}$ −45 (*c* 1.0, $CHCl_3$). IR (film, $CHCl_3$) ν (cm^{-1}): 1374 and 1670. ^{1}H NMR ($CDCl_3$, 300 MHz) δ 1.29 (s, 3H, CH_3), 1.45 (s, 3H, CH_3), 1.62−1.70 (m, 2H, H-4a), 1.72−1.80 (m, 2H, H-3a), 2.16−2.23 (m, 2H, H-2a), 2.36−2.41 (m, 2H, H-5a), 3.38 (s, 3H, OCH_3), 4.40 (dd, 1H, J = 5.9 and 9.9 Hz, H-3′), 4.50−4.59 (m, 2H, H-5′), 4.66 (d, 1H, J = 5.9 Hz, H-4′), 4.74 (d, 1H, J = 5.8 Hz, H-2′), 5.00 (s, 1H, H-1′), 6.51−6.53 (m, 1H, H-6a), 7.48 (s, 1H, H-5 triazole). ^{13}C NMR ($CDCl_3$, 75 MHz) δ 22.0 (C-4a), 22.2 (C-2a and C-1a), 24.7 (CH_3), 25.0 (C-5a), 26.1 (CH_3), 52.7 (C-5′), 55.3 (OCH_3), 81.6 (C-3′), 84.8 (C-4′), 85.0 (C-2′), 109.9 (C-1′), 112.6 (C-6′), 124.9 (C-6a and C-5), 127.0 (C-Ar-1a), 151.1 (C-4). HRMS (EI) calcd for $C_{17}H_{25}N_3O_4$: 335.1845. Found: 336.4104 $(M + H)^+$. Anal. Calcd for $C_{17}H_{25}N_3O_4$: C, 60.88; H, 7.51; N, 12.53. Found: C, 60.87; H, 7.49; N, 12.51.

1-*O*-Methyl-2,3-*O*-isopropylidene-5-(4-hydroxymethyl-1*H*-1,2,3-triazol-1-yl)-β-D-ribofuranose (4c). Compound **4c** was obtained as a light-yellowish powder in 80% yield. Mp 93−95 °C. $[\alpha]_{20}^{D}$ −16 (*c* 1.0, $CHCl_3$). IR (film, $CHCl_3$) ν (cm^{-1}): 3452 and 1654. ^{1}H NMR ($CDCl_3$, 300 MHz) δ 1.30 (s, 3H, CH_3), 1.45 (s, 3H, CH_3), 1.70 (s, 1H, OH), 3.39 (s, 3H, OCH_3), 4.39−4.46 (m, 1H, H-3′), 4.51−4.61 (m, 2H, H-5′), 4.66 (d, 1H, J = 5.8 Hz, H-3′), 4.74 (d, 1H, J = 5.8 Hz, H-2′), 4.79 −4.80 (m, 2H, H-1a), 5.01 (s, 1H, H-1′), 7.64 (s, 1H, H-5). ^{13}C NMR ($CDCl_3$, 75 MHz) δ 25.1 (CH_3), 26.5 (CH_3), 53.3 (C-5′), 55.8 (OCH_3), 56.4 (C-1a), 82.0 (C-2′), 85.2 (C-3′), 85.2 (C-3′), 85.4 (C-4′), 110.2 (C-1′), 113.1 (C-6′), 122.4 (C-5), 148.3 (C-4). HRMS (EI) calcd for $C_{12}H_{19}N_3O_5$: 285.1325. Found: 286.3085 $(M + H)^+$. Anal. Calcd for $C_{12}H_{19}N_3O_5$: C, 50.52; H, 6.21; N, 14.73. Found: C, 50.53; H, 6.23; N, 14.70.

1-*O*-Methyl-2,3-*O*-isopropylidene-5-(4-carboxylate ethyl-1*H*-1,2,3-triazol-1-yl)-β-D-ribofuranose (4d). Compound **4d** was obtained as a white powder in 87% yield. Mp 88−90 °C. $[\alpha]_{20}^{D}$ −44 (*c* 1.0, $CHCl_3$). IR (film, $CHCl_3$) ν (cm^{-1}): 2931 and 1730. ^{1}H NMR ($CDCl_3$, 300 MHz) δ 1.30 (s, 3H, CH_3), 1.41 (t, 3H, J = 7.0 Hz, C-3a-CH_3), 1.45 (s, 3H, CH_3), 3.37 (s, 3H, OCH_3), 4.39 − 4.63 (m, 5H, H-4′, H-5′, H-2a), 4.66 (d, 1H, J = 5.8 Hz, H-3′), 4.73 (d, 1H, J = 5.8 Hz, H-2′), 5.00 (s, 1H, H-1′), 8.23 (s, 1H, H-5). ^{13}C NMR ($CDCl_3$, 75 MHz) δ 14.1 (C-3a), 24.7 (CH_3), 26.1 (CH_3), 53.2 (C-5′), 55.5 (OCH_3), 61.1 (C-2a), 81.4 (C-2′), 84.7 (C-3′), 84.9 (C-4′), 109.0 (C-1′), 112.2 (C-6′), 112.2 (C-4), 109.6 (C-5), 159.6 (C=O). HRMS (EI) calcd for $C_{14}H_{21}N_3O_6$: 327.1430. Found: 328.3453 $(M + H)^+$. Anal. Calcd for $C_{14}H_{21}N_3O_6$: C, 51.37; H, 6.47; N, 12.84. Found: C, 51.31; H, 6.45; N, 12.89.

1-*O*-Methyl-2,3-*O*-isopropylidene-5-(4-phenoxymethyl-1*H*-1,2,3-triazol-1-yl)-β-D-ribofuranose (4e). Compound **4e** was obtained as a light-yellowish powder in 80% yield. Mp 80−83 °C. $[\alpha]_{20}^{D}$ −28 (*c* 1.0, $CHCl_3$). IR (film, $CHCl_3$) ν (cm^{-1}): 3065 and 1595. ^{1}H NMR ($CDCl_3$, 300 MHz) δ 1.30 (s, 3H, CH_3), 1.45 (s, 3H, CH_3), 3.36 (s, 3H, OCH_3), 4.41−4.46 (m, 1H, H-4′), 4.54−4.61 (m, 2H, H-5′), 4.66 (d, 1H, J = 5.8 Hz, H-3′), 4.75 (d, 1H, J = 5.8 Hz, H-2′), 5.00 (s, 1H, H-1′), 5.22 (s, 2H, H-1a), 6.97−7.00 (m, 3H, H-4a and H-5a), 7.26−7.31 (m, 2H, H-2a and H-3a), 7.70 (s, 1H, H-5). ^{13}C NMR ($CDCl_3$, 75 MHz) δ 25.1 (CH_3), 26.6 (CH_3), 53.4 (C-5′), 55.8 (OCH_3), 62.2 (C-1a), 82.0 (C-4′), 85.2 (C-3′), 85.4 (C-2′), 110.3 (C-1′), 113.2 (C-6′), 115.0 (C-3a), 121.5 (C-5a), 123.9 (C-5), C-4 not observed, 159.6 (C=O). HRMS (EI) calcd for $C_{18}H_{23}N_3O_5$: 361.1638. Found: 362.4054 $(M + H)^+$. Anal. Calcd for $C_{18}H_{23}N_3O_5$: C, 59.82; H, 6.41; N, 11.63. Found: C, 59.85; H, 6.40; N, 11.65.

1-*O*-Methyl-2,3-*O*-isopropylidene-5-[4-(3-chloropropyl)-1*H*-1,2,3-triazol-1-yl]-β-D-ribofuranose (4f). Compound **4f** was obtained as a white powder in 90% yield. Mp 60−63 °C. $[\alpha]_{20}^{D}$ −56 (*c* 1.0, $CHCl_3$). IR (film, $CHCl_3$) ν (cm^{-1}): 2987 and 1632. ^{1}H NMR ($CDCl_3$, 300 MHz) δ 1.29 (s, 3H, CH_3), 1.44 (s, 3H, CH_3), 2.17 (q, 2H, J = 6.6 and 7.3 Hz, H-2a), 2.89 (t, 2H, J = 7.6 Hz, H-1a), 3.38 (s, 3H, OCH_3), 3.57 (t, 2H, J = 6.6 Hz, H-3a), 4.37−4.43 (m, 1H, H-4′), 4.50−4.59 (m, 2H, H-5′), 4.65 (d, 1H, J = 5.8 Hz, H-3′), 4.74 (d, 1H, J = 5.8 Hz, H-2′), 5.00 (s, 1H, H-1′), 7.43 (s, 1H, H-5). ^{13}C NMR ($CDCl_3$, 75 MHz) δ 22.4 (C-1a), 24.7 (CH_3), 26.1 (CH_3), 31.5 (C-2a), 43.9 (C-3a), 52.84 (C-5′), 55.3 (OCH_3), 81.6 (C-3′), 84.8 (C-4′), 85.0 (C-2′), 109.6 (C-5), 109.8 (C-1′), 112.7 (C-6′), 112.5(C-4). HRMS (EI) calcd for $C_{14}H_{22}ClN_3O_4$: 331.1299. Found: 332.8078 $(M + H)^+$. Anal. Calcd for $C_{14}H_{22}ClN_3O_4$: C, 50.68; H, 6.68; N, 12.66. Found: C, 50.70; H, 6.70; N, 12.67.

1-*O*-Methyl-2,3-*O*-isopropylidene-5-[4-(1-hydroxycyclohexil)-1*H*-1,2,3-triazol-1-yl]-β-D-ribofuranose (4g). Compound **4g** was obtained as a white powder in 88% yield. Mp 113−115 °C. $[\alpha]_{20}^{D}$ −48 (*c* 1.0, $CHCl_3$). IR (film, $CHCl_3$) ν (cm^{-1}): 3421 and 2935. ^{1}H NMR ($CDCl_3$, 300 MHz) δ 1.29 (s, 3H, CH_3), 1.45 (s, 3H, CH_3), 1.57−2.00 (m, 4H, H-2a, 3a, 4a, and 5a), 2.39 (s, 1H, O-H), 3.38 (s, 3H, OCH_3), 4.35−4.38 (m, 1H, H-4′), 4.44−4.59 (m, 2H, H-5′), 4.65 (d, 1H, J = 5.8 Hz, H-3′), 4.75 (d, 1H, J = 5.8 Hz, H-2′), 5.00 (s, 1H, H-1′), 7.57 (s, 1H, H-5). ^{13}C NMR ($CDCl_3$, 75 MHz) δ 21.7 (C-3a), 24.7 (CH_3), 25.2 (C-4a), 26.2 (CH_3), 37.9 (C-2a), 53.0 (C-5′), 55.4 (OCH_3), 81.7 (C-3′), 84.8 (C-4′), 85.0 (C-2′), 109.9 (C-1′), 112.7 (C-6′), 115.6 (C-5), C-4, not observed. HRMS (EI) calcd for $C_{17}H_{27}N_3O_5$: 353.1951. Found: 354.4267 $(M + H)^+$. Anal. Calcd for $C_{17}H_{27}N_3O_5$: C, 57.77; H, 7.70; N, 11.89. Found: C, 57.79; H, 7.71; N, 11.84.

1-*O*-Methyl-2,3-*O*-isopropylidene-5-[4-(1-hydroxy-1-methyl-ethyl)-1*H*-1,2,3-triazol-1-yl]-β-D-ribofuranose (4h). Compound **4h** was obtained as a white powder in 79% yield. Mp 104−106 °C. $[\alpha]_{20}^{D}$ −27 (*c* 1.0, $CHCl_3$). IR (film, $CHCl_3$) ν (cm^{-1}): 3461. ^{1}H NMR ($CDCl_3$, 300 MHz) δ 1.30 (s, 3H, CH_3), 1.45 (s, 3H, CH_3), 1.64 (s, 6H, 2 CH_3), 2.47 (s, 1H, O−H), 3.39 (s, 3H, OCH_3), 4.38−4.44 (m, 1H, H-4′), 4.51−4.60 (m, 2H, H-5′), 4.66 (d, 1H, J = 5.8 Hz, H-3′), 4.74 (d, 1H, J = 5.8 Hz, H-2′), 5.00 (s, 1H, H-1′), 7.54 (s, 1H, H-5). ^{13}C NMR ($CDCl_3$, 75 MHz) δ 24.7 (CH_3), 26.2 (CH_3), 30.2 (CH_3), 30.3 (CH_3), 52.0 (C-5′), 55.4 (OCH_3), 68.3 (C-1a), 81.6 (C-3′), 84.2 (C-4′), 85.0 (C-2′), 109.9 (C-1′), 112.2 (C-6′), 119.3 (C-5), 161.3 (C-4). HRMS (EI) calcd $C_{14}H_{23}N_3O_5$: 313.1638. Found: 314.3611 $(M + H)^+$. Anal. Calcd for $C_{14}H_{23}N_3O_5$: C, 53.66; H, 7.40; N, 13.41. Found: C, 53.65; H, 7.40; N, 13.43.

1-*O*-Methyl-2,3-*O*-isopropylidene-5-(4-propyl-1*H*-1,2,3-triazol-1-yl)-β-D-ribofuranose (4i). Compound **4i** was obtained as a white powder in 85% yield. Mp 106−107 °C. $[\alpha]_{20}^{D}$ −24 (*c* 1.0, $CHCl_3$). IR (film, $CHCl_3$) ν (cm^{-1}): 2939 and 2986. ^{1}H NMR ($CDCl_3$, 300 MHz) δ 1.30 (s, 3H, CH_3), 1.40 (t, 3H, J = 7.5 Hz, CH_3), 1.45 (s, 3H, CH_3), 3.38 (s, 3H, OCH_3), 4.39−4.63 (m, 7H, H-4′, H-5′ and H-2a and 1a), 4.66 (d, 1H, J = 5.8 Hz, H-3′), 4.73 (d, 1H, J = 5.8 Hz, H-2′), 5.01 (s, 1H, H-1′), 8.19 (s, 1H, H-5). ^{13}C NMR ($CDCl_3$, 75 MHz) δ 14.13 (C-3a), 19.2 (C-2a), 24.7 (CH_3), 26.1 (CH_3), 26.0 (C-1a), 53.2 (C-5′), 55.5 (OCH_3), 81.4 (C-3′), 84.8 (C-4′), 84.7 (C-2′), 110.0 (C-1′), 112.0 (C-6′), 127.6 (C-5), 140.3 (C-4). HRMS (EI) calcd $C_{14}H_{23}N_3O_4$: 297.1689. Found: 298.2611

$(M + H)^+$. Anal. Calcd for $C_{14}H_{23}N_3O_4$: C, 56.55; H, 7.80; N, 14.13. Found: C, 56.57; H, 7.82; N, 14.15.

1-*O*-Methyl-2,3-*O*-isopropylidene-5-[4-(1-hydroxy-1-methylpropyl)-1*H*-1,2,3-triazol-1-yl]-β-D-ribofuranose (4j). Compound **4j** was obtained as a white powder in 84% yield. Mp 111−113 °C. $[\alpha]_{20}^{D}$ −41 (*c* 1.0, $CHCl_3$). IR (film, $CHCl_3$) ν (cm^{-1}): 3355, 2970, and 2936. ^1H NMR ($CDCl_3$, 300 MHz) δ 0.85 (t, 3H, *J* = 7.3 Hz, C-3a), 1.30 (s, 3H, CH_3), 1.45 (s, 3H, CH_3), 1.57 (s, 3H, C-4a), 2.49 (s, 1H, O−H), 3.38 (s, 3H, OCH_3), 4.35−4.44 (m, 1H, H-4′), 4.51−4.58 (m, 2H, H-5′), 4.64 (d, 1H, *J* = 5.8 Hz, H-3′), 4.75 (d, 1H, *J* = 5.8 Hz, H-2′), 5.01 (s, 1H, H-1′), 7.52 (s, 1H, H-5). ^{13}C NMR ($CDCl_3$, 75 MHz) δ 8.0 (C-3a), 24.7 (CH_3), 26.2 (CH_3), 27.7 (C-4a), 35.7 (C-2a), 52.9 (C-5′), 55.3 (OCH_3), 71.0 (C-1a), 81.6 (C-3′), 84.8 (C-4′), 85.0 (C-2′), 109.9 (C-1′), 112.2 (C-6′), 120.0 (C-5), 154.6 (C-4). HRMS (EI) calcd $C_{15}H_{25}N_3O_5$: 327.1794. Found: 328.3889 $(M + H)^+$. Anal. Calcd for $C_{15}H_{25}N_3O_5$: C, 55.03; H, 7.70; N, 12.84. Found: C, 55.06; H, 7.73; N, 12.86.

1-*O*-Methyl-2,3-*O*-isopropylidene-5-(4-methylacetate-1*H*-1,2,3-triazole-1-yl)-β-D-ribofuranose (4l). Compound **4l** was obtained as light-yellowish powder in 85% yield. Mp 73−74 °C. $[\alpha]_{20}^{D}$ −23 (*c* 1.0, $CHCl_3$). IR (film, $CHCl_3$) ν (cm^{-1}): 2987, 2941, and 1740. ^1H NMR ($CDCl_3$, 300 MHz) δ 1.27 (s, 3H, CH_3), 1.42 (s, 3H, s, CH_3), 2.04 (s, 3H, C-3a), 3.35 (s, 3H, OCH_3), 4.34−4.43 (m, 1H, H-4′), 4.53−4.58 (m, 2H, H-5′), 4.62 (d, 1H, *J* = 5.8 Hz, H-3′), 4.73 (d, 1H, *J* = 5.8 Hz, H-2′), 4.98 (s, 1H, H-1′), 5.18 (s, 1H, C-1a), 7.69 (s, 1H, H-5). ^{13}C NMR ($CDCl_3$, 75 MHz) δ 20.6 (C-3a), 24.7 (CH_3), 26.1 (CH_3), 52.9 (C-5′), 55.4 (OCH_3), 57.3 (C-1a), 81.5 (C-3′), 84.7 (C-4′), 84.9 (C-2′), 109.9 (C-1′), 112.7 (C-6′), 123.9 (C-5), 142.8 (C-4), 170.6 (C═O). HRMS (EI) calcd $C_{14}H_{21}N_3O_6$: 327.1430. Found: 328.3453 $(M + H)^+$. Anal. Calcd for $C_{14}H_{21}N_3O_6$: C, 51.37; H, 6.47; N, 12.84. Found: C, 51.38; H, 6.49; N, 12.86.

1-*O*-Methyl-2,3-*O*-isopropylidene-5-[4-(tetrahydro-2*H*-pyran)-methyl)-1*H*-1,2,3-triazole-1-yl]-β-D-ribofuranose (4m). Compound **4m** was obtained as a white powder in 95% yield. Mp 63−66 °C. $[\alpha]_{20}^{D}$ −25 (*c* 1.0, $CHCl_3$). IR (film, $CHCl_3$) ν (cm^{-1}): 2942 and 2873. ^1H NMR ($CDCl_3$, 300 MHz) δ 1.29 (s, 3H, CH_3), 1.44 (s, 3H, CH_3), 1.50−1.84 (m, 6H, C-3a, C-4a, C-5a), 3.38 (s, 3H, OCH_3), 3.56−3.58 (m, 1H, C-6a), 3.86−3.92 (m, 1H, C-6a), 4.36 − 4.42 (m, 1H, H-4′), 4.52−4.67 (m, 4H, H-5′ and C-2a), 4.73−4.76 (m, 1H, H-3′), 4.73 (d, 1H, *J* = 5.8 Hz, H-2′), 5.01 (s, 1H, H-1′), 7.64 (s, 1H, H-5). ^{13}C NMR ($CDCl_3$, 75 MHz) δ 19.1 (C-4a), 24.7 (CH_3), 25.1 (C-5a), 26.1 (CH_3), 30.2 (C-3a), 52.8 (C-5′), 55.3 (OCH_3), 60.3 (C-1a), 62.1 (C-6a), 81.6 (C-3′), 84.8 (C-4′), 85.0 (C-2′), 98.0 (C-2a), 109.8 (C-1′), 112.6 (C-6′), 122.6 (C-5), 145.3 (C-4). HRMS (EI) calcd $C_{17}H_{27}N_3O_6$: 369.1408. Found: 370.4258 $(M + H)^+$. Anal. Calcd for $C_{17}H_{27}N_3O_6$: C, 55.27; H, 7.37; N, 11.37. Found: C, 55.25; H, 7.35; N, 11.35.

1-*O*-Methyl-2,3-*O*-isopropylidene-5-[4-(1-hydroxy-1,3-dimethylbutyl)-1*H*-1,2,3-triazole-1-yl]-β-D-ribofuranose (4n). Compound **4n** was obtained as a white powder in 79% yield. Mp 79−81 °C. $[\alpha]_{20}^{D}$ −32 (*c* 1.0, $CHCl_3$). IR (film, $CHCl_3$) ν (cm^{-1}): 3421, 2951, and 2873. ^1H NMR ($CDCl_3$, 300 MHz) δ 0.83 (d, 3H, *J* = 6,5 Hz, C-4a), 0.86 (d, 3H, *J* = 6.5 Hz, C-5a), 1.30 (s, 3H, CH_3), 1.45 (s, 3H, CH_3), 1.61 (s, 3H, C-6a), 1.66−1.86 (m, 3H, C-2a and C-3a), 2.33 (s, 1H, OH), 3.38 (s, 3H, OCH_3), 4.37 − 4.45 (m, 1H, H-4′), 4.51−4.60 (m, 2H, H-5′), 4.66 (d, 1H, *J* = 5.8 Hz, H-3′), 4.74 (dd, 1H, *J* = 2.4 and 5.8 Hz, H-2′), 5.01 (s, 1H, H-1′), 7.53 (s, 1H, H-5). ^{13}C NMR ($CDCl_3$, 75 MHz) δ 24.1 (C-4a), 24.1 (C-5a), 24.2 (C-6a), 24.7 (CH_3), 26.1 (CH_3), 29.1 (C-3a), 51.4 (C-5′), 52.9 (C-2a), 55.3 (OCH_3), 71.2 (C-1a), 81.6 (C-3′), 84.1 (C-4′), 84.9 (C-2′), 109.9 (C-1′), 112.2 (C-6′), 119.9 (C-5), 135.7 (C-4). HRMS (EI) calcd $C_{17}H_{29}N_3O_5$: 355.2107. Found: 356.4420 $(M + H)^+$. Anal. Calcd for $C_{17}H_{29}N_3O_5$: C, 57.45; H, 8.22; N, 11.82. Found: C, 57.47; H, 8.25; N, 11.85.

1,2:3,4-Di-*O*-isopropylidene-6-(4-phenyl-1*H*-1,2,3-triazole-1-yl)-α-D-galactopyranose. (5a). Compound **5a** was obtained as a white powder in 90% yield. Mp 152−154 °C. $[\alpha]_{20}^{D}$ −98 (*c* 1.0, $CHCl_3$). IR (film, $CHCl_3$) ν (cm^{-1}): 2987 and 2932. ^1H NMR ($CDCl_3$, 300 MHz) δ 1.29 (s, 3H, CH_3), 1.37 (s, 3H, CH_3), 1.40 (s, 3H, CH_3), 1.57 (s, 3H, CH_3), 4.21−4.26 (m, 2H, H-6′), 4.34 (q, 1H, *J* = 4.8 Hz, H-2′), 4.45−4.53 (m, 1H, H-3′), 4.63−4.71 (m, 2H, H-5′and H-4′), 5.54 (d, 1H, *J* = 4.8 Hz, H-1′), 7.29−7.34 (m, 1H, H-3a), 7.39−7.44 (m, 2H, H-2a), 7.82−7.85 (m, 2H, H-1a), 7.95 (s, 1H, H-5). ^{13}C NMR ($CDCl_3$, 75 MHz) δ 24.6 (CH_3), 25.1 (CH_3), 26.2 (CH_3), 26.2 (CH_3), 50.8 (C-6′), 67.5 (C-5′), 70.6 (C-2′), 71.0 (C-3′), 71.4 (C-4′), 96.5 (C-1′), 109.3 (C-7′), 110.1 (C-8′), 121.1 (C-5), 126.0 (C-1a), 128.2 (C-3a), 129.0 (C-2a), 131.0 (C-ar), 147.7 (C-4). HRMS (EI) calcd $C_{20}H_{25}N_3O_5$: 387.1794. Found: 388.4431 $(M + H)^+$. Anal. Calcd for $C_{20}H_{25}N_3O_5$: C, 62.00; H, 6.50; N, 10.85. Found: C, 62.03; H, 6.53; N, 10.87.

1,2:5,6-Di-*O*-isopropylidene-3-(4-phenyl-1*H*-1,2,3-triazole-1-yl)-α-D-alofuranose (6a). Compound **6a** was obtained as a white powder in 89% yield. Mp 155−157 °C. $[\alpha]_{20}^{D}$ −87 (*c* 1.0, $CHCl_3$). IR (film, $CHCl_3$) ν (cm^{-1}): 2987 and 2935. ^1H NMR ($CDCl_3$, 300 MHz) δ 1.32 (s, 3H, CH_3), 1.36 (s, 3H, CH_3), 1.43 (s, 3H, CH_3), 1,51 (3H, s, CH_3), 3.90−4.00 (m, 2H, H4′ and H-5′), 4.20−4.28 (m, 2H, H-6′), 4.33−4.38(m, 1H, H-3′), 5.03 (d, 1H, *J* = 3.6 Hz, H-2′), 6.27 (1H, d, *J* = 3,4 Hz, H-1′), 7.29−7.34 (m, 1H, H-3a), 7.32−7.37 (m, 1H, H-3a), 7.40−7.46 (m, 2H, H-2a), 7.82−7.85 (m, 2H, H-1a), 7.91 (s, 1H, H-5). ^{13}C NMR ($CDCl_3$, 75 MHz) δ 25.0 (CH_3), 26.0 (CH_3), 26.5 (CH_3), 26.7 (CH_3), 66.2 (C-3′), 67.5 (C-6′), 72.9 (C-4′), 80.4 (C-5′), 83.3 (C-2′), 104.9 (C-1′), 106.2 (C-7′), 109.4 (C-8′), 112.2 (C-5), 125.6 (C-1a), 128.7 (C-2a), 128.1 (C-ar), 130.2 (C-4). HRMS (EI) calcd $C_{20}H_{25}N_3O_5$: 387.1794. Found: 388.4431 $(M + H)^+$. Anal. Calcd for $C_{20}H_{25}N_3O_5$: C, 62.00; H, 6.50; N, 10.85. Found: C, 62.01; H, 6.52; N, 10.86.

5-Deoxy-1,2-*O*-isopropylidene-5-(4-phenyl-1*H*-1,2,3-triazole-1-yl)-α-D-xylofuranose (7a). Compound **7a** was obtained as a light-yellowish powder. Yield: 97%. Mp 50−53 °C. $[\alpha]_{20}^{D}$ −17 (*c* 1.0, $CHCl_3$). IR (film, $CHCl_3$) ν (cm^{-1}): 3419 and 2861. ^1H NMR ($CDCl_3$, 300 MHz) δ 1.32 (s, 3H, CH_3), 1.50 (s, 3H, CH_3), 2.00 (s, 1H, OH), 4.33 (dd, 1H, *J* = 4.9 Hz, H-3′), 4.51−4.65(m, 3H, H-4′ and H-5′), 4.84 (dd, 1H, *J* = 5.1 Hz, H-2′), 6.01 (d, 1H, *J* = 3.6 Hz, H-1′), 7.33−7.46 (m, 3H, H-2a and 4a), 7.75−7.80 (m, 3H, H-3a and H-5). ^{13}C NMR ($CDCl_3$, 75 MHz) δ 26.4 (CH_3), 26.9 (CH_3), 49.4 (C-5′), 75.4 (C-2′), 78.6 (C-3′), 85.6 (C-4′), 105.0 (C-1′), 112.2 (C-6′), 120.2 (C-5), 124.0 (C-1a), 128.1 (C-2a), 130.3 (C-3a and 4a), 128.7 (C-2a), 128.1 (C-ar), 156.4 (C-4). HRMS (EI) calcd $C_{16}H_{17}N_3O_5$: 317.1376. Found: 318.3526 $(M + H)^+$. Anal. Calcd for $C_{16}H_{19}N_3O_4$: C, 60.56; H, 6.03; N, 13.24. Found: C, 60.57; H, 6.05; N, 13.25.

5-Deoxy-1,2-*O*-isopropylidene-5-[4-(1-cyclohexene)-1*H*-1,2,3-triazole-1-yl]-α-D-xylofuranose (7b). Compound **7b** was obtained as a light-yellowish powder in 98% yield. Mp 140−142 °C. $[\alpha]_{20}^{D}$ −15 (*c* 1.0, $CHCl_3$). IR (film, $CHCl_3$) ν (cm^{-1}): 3270 and 2931. ^1H NMR ($CDCl_3$, 300 MHz) δ 1.30 (s, 3H, CH_3), 1.44 (s, 3H, CH_3), 1.63−1.70 (m, 2H, H-4a), 1.72−1.79 (m, 2H, H-6a), 2.17−2.23 (m, 2H, H-5a), 2.35−2.40 (m, 2H, H-3a), 3.80−3.82 (m, 1H, H-3′), 4.18−4.21 (m, 1H, OH), 4.39−4.53 (m, 2H, H-5′), 4.58 (d, 1H, *J* = 3.4 Hz, H-2′), 4.74−4.81 (m, 1H, H-4′), 5.96 (d, 1H, *J* = 3.4 Hz, H-1′), 6.46−6.50 (m, 1H, H-2a), 7.51 (s, 1H, H-5). ^{13}C NMR ($CDCl_3$, 75 MHz) δ 22.3 (C-4a and C-5a), 22.6 (C-3a), 25.5 (C-6a), 26.4 (CH_3), 26.5 (C-3a), 27.0 (CH_3), 49.2 (C-5′), 74.4 (C-3′), 79.7 (C-2′), 85.6 (C-4′), 105.4 (C-1′), 112.1 (C-6′), 120.2 (C-1a), 125.8 (C-2a), 127.2 (C-5), 149.7 (C-4). HRMS (EI) calcd $C_{16}H_{23}N_3O_4$: 321.1689. Found: 322.3853 $(M + H)^+$. Anal. Calcd for $C_{16}H_{23}N_3O_4$: C, 59.80; H, 7.21; N, 13.08. Found: C, 59.83; H, 7.23; N, 13.09.

5-Deoxy-1,2-*O*-isopropylidene-5-(4-hydroxymethyl-1*H*-1,2,3-triazole-1-yl)-α-D-xylofuranose (7c). Compound **7c** was obtained as a white powder in 75% yield. Mp 50−51 °C. $[\alpha]_{20}^{D}$ −35 (*c* 1.0, $CHCl_3$). IR (film, $CHCl_3$) ν (cm^{-1}): 3448, 2986, and 2936. ^1H NMR ($CDCl_3$, 300 MHz) δ 1.32 (s, 3H, CH_3), 1.50 (s, 3H, CH_3), 2.88 (s, 1H, H-1a), 2.96 (s, 1H, H-1a), 3.55−3.67 (m, 2H, H-3′ and 4′), 4.24−4.31 (m, 2H, H-5′), 4.53 (d, 1H, *J* = 3.6 Hz, H-2′), 5.94 (d, 1H, *J* = 3.6 Hz, H-1′), 8.00 (s, 1H, H-5). ^{13}C NMR ($CDCl_3$, 75 MHz) δ 26.9 (CH_3), 26.5 (CH_3), 48.5 (C-1a), 49.0 (1H, C-5′), 74.8 (C-3′), 78.73 (C-2′), 85.1 (C-4′), 105.4 (C-1′), 104.6 (C-6′), 127.7 (C-5), 129.9 (C-4). HRMS (EI)

calcd $C_{11}H_{17}N_3O_5$: 271.1168. Found: 238.0905 $(M + H)^+$. Anal. Calcd for $C_{11}H_{17}N_3O_5$: C, 48.70; H, 6.32; N, 15.49. Found: C, 48.72; H, 6.33; N, 15.51.

Biochemistry. The α-glucosidase inhibitory activity was assayed using the yeast maltase enzyme (Sigma-Aldrich, St. Louis, MO) according to the procedure described by Matsui and collaborators.[44] The α-glucosidase activity was determined by monitoring the *p*-nitrophenol released from *p*-nitrophenyl-α-D-glycopyranoside at 405 nm. The compounds in the series under study were first screened for α-glucosidase inhibition at a fixed concentration of 500 μM, and activities were expressed as percentage inhibitions relative to a control assay with no inhibitor added. Compounds showing the highest inhibitory activities were further characterized by determining the concentration required to inhibit 50% of the α-glucosidase activity under the assay conditions (defined as the IC_{50} value). Acarbose (Glucobay, Bayer) was used in the assays for comparison.

Pharmacology. The animals (male Wistar rats, 2−3 months old, 200−250 g) were divided into four groups of five rats each. Group 1 consisted of nondiabetic control rats that received a physiological NaCl solution containing DMSO at 1% (as vehicle). Group 2 received acarbose (50 mg/kg), group 3 received triazole **4a** (50 mg/kg), and group 4 received triazole **4e** (50 mg/kg) in the same vehicle. Following the general procedure of Kanthi and collaborators,[45] each triazole or acarbose was suspended in 0.5 mL of physiological NaCl solution containing DMSO at 1% and administered orally by a cannula to 8 h fasted rats 5 min before the oral administration of 1 mL of maltose (3 g/kg). The control group was given the same volume of vehicle before the maltose solution. Blood samples were obtained from the tail vein 5 min before the oral administration of the drugs or the vehicle (T_0) and at 30, 60, and 120 min thereafter. Glucose concentration was measured in total blood with an Accu-check compact machine (Roche). Data were expressed as the mean ± SD. Significant differences between sample and control groups were examined with Dunnett's *t*-test ($n = 5$, (∗) $P < 0.05$).

Molecular Modeling. MAL12 Model Building and Validation. Homology modeling of MAL12 was carried out using the Modeller software, version 9v2,[46] based on the crystal structures of *B. cereus* oligo-α-1,6-glucosidase (PDB code 1UOK, 2.0 Å resolution, 39% identity among 581 aligned residues)[47] and of *Geobacillus* sp. α-glucosidase GSJ (PDB code 2ZE0, 2.0 Å resolution, 39% identity among 591 aligned residues).[36] The target sequence was found at the UniprotKB/Swiss-Prot database under access number P53341, and the sequence alignment was performed using the T-Coffee server.[48] A set of 50 modeled structures was generated and ranked by the Modeller objective function and the top-scoring models were checked for their stereochemical and overall structural quality, using the ProCheck,[34] Verify-3D,[35] and Whatcheck[49] computer programs. A single model was selected for further analysis and as a starting structure for docking simulations.

Defining the Binding Site on MAL12. According to the DALI server (DALI, version 3),[50] the 3D structure of *T. maritima* 4-α-glucanotransferase in complex with modified acarbose (PDB code 1LWJ, 2.50 Å resolution)[35] shows significant folding similarity, although low sequence identity, with 1UOK (1.45 Å rmsd over 317 Cα atoms and 27% of identity) and 2ZE0 (1.52 Å rmsd over 305 Cα atoms and 29% of identity). Additionally, the catalytic residues and some of the residues important for substrate binding are highly conserved in all members of the GH13 family. Thus, the definition of the putative binding site for acarbose in MAL12 was based on the structural similarity with the homologous residues in 1LWJ involved in the binding of modified acarbose as found in the complex. The same binding site was used to perform the molecular docking of the triazoles. The MAL12/acarbose complex was effectively generated by superposing the MAL12 modeled structure onto 1LWJ and then transferring the acarbose atomic coordinates to the MAL12 model using the Sybyl molecular modeling package, version 8.0 (Tripos Associates, St. Louis, MO). The hydrogen atoms were added to the protein and ligand structures, and 1000 steps of energy minimization were performed by the steepest descent method, using Gasteiger−Hückel charges and a dielectric constant of 80, in the Tripos force field.

Molecular Docking of the 1,2,3-Glucotriazoles. The molecular models of the 1,2,3-glucotriazoles were built using the Sybyl molecular modeling package, version 8.0 (Tripos Associates, St. Louis, MO). The hydrogen atoms were added to the structures, and 1000 steps of energy minimization were performed by the steepest descent method, using Gasteiger−Hückel charges and a dielectric constant of 80, in the Tripos force field. The structures were further optimized using the conjugated gradient method. Ligand−protein docking was performed with the molecular docking algorithm MolDock[51] using the Molegro Virtual Docker software, version 3.0.0 (Molegro ApS, Aarhus, Denmark, http://www.molegro.com). MolDock uses a heuristic search algorithm (termed guided differential evolution) which is a combination of differential evolution and a cavity-prediction algorithm. The docking scoring function is an extension of the piecewise linear potential (PLP).[51] After the ligands and the protein coordinates were imported, all structural parameters including bond type, hybridization, explicit hydrogen, charges, and flexible torsions were assigned using the automatic preparation function in Molegro Virtual Docker software, version 3.0.0.[51] For each compound, 50 docking runs were performed with the initial population of 300 individuals. The software is also able to work with side chain conformational changes by softening the potentials (steric, hydrogen bonds, and electrostatic force) used during a docking simulation. The residues considered flexible were those that were close enough to the reference ligand to interact with it (6 Å around the acarbose, 69 residues). After each ligand had been docked, the side chains chosen were energy-minimized by the Molegro Virtual Docker software, version 3.0.0,[51] with respect to the conformation found, using the standard nonsoftened potentials. Only torsion angles in the side chains were modified during the minimization; all other properties (including bond lengths and backbone atom positions) were held fixed.[51] In order to identify which of the ligand configurations most likely represented the correct binding mode of the triazole compounds, all complexes were analyzed considering evidence from sequence conservation, visual inspection, and automated assignment of interatomic contacts using the Ligplot program and the CSU/LPC server.[52]

Acknowledgment. This research was supported by grants from CNPq (National Council of Research of Brazil), CAPES, FAPERJ (PRONEX E-26/171.512/2006), UFRJ, UFAM, Fiocruz, and UFF for contribution to the funding of this program.

Supporting Information Available: Experimental procedures and characterization data for azido derivatives and the precursors derivatives; results of the analysis of all 1*H*-1,2,3-triazoles synthesized and evaluated in this study (^{1}H NMR, ^{13}C NMR, and mass spectra). This material is available free of charge via the Internet at http://pubs.acs.org.

References

(1) Dwek, R. A. Glycobiology: toward understanding the function of sugars. *Chem. Rev.* **1996**, *96*, 683–720.
(2) Tattersall, R. Alpha-glucosidase inhibition as an adjunct to the treatment of type-1 diabetes. *Diabetic Med.* **1993**, *10*, 688–693.
(3) Sim, L.; Quezada-Calvillo, R.; Sterchi, E. E.; Nichols, B. L.; Rose, D. R. Human intestinal maltase−glucoamylase: crystal structure of the N-terminal catalytic subunit and basis of inhibition and substrate specificity. *J. Mol. Biol.* **2008**, *375*, 782–792.
(4) Henrissat, B. A Classification of glycosyl hydrolases based on amino-acid-sequence similarities. *Biochem. J.* **1991**, *280*, 309–316.
(5) Henrissat, B.; Bairoch, A. Updating the sequence-based classification of glycosyl hydrolases. *Biochem. J.* **1996**, *316*, 695–696.

(6) Henrissat, B.; Callebaut, I.; Fabrega, S.; Lehn, P.; Mornon, J-P; Davies, G. Conserved catalytic machinery and the prediction of a common fold for several families of glycosyl hydrolases. *Proc. Natl. Acad. Sci. U.S.A.* **1995**, *92*, 7090–7094.

(7) Stam, M. R.; Danchin, E. G. J.; Rancurel, C.; Coutinho, P. M.; Henrissat, B. Dividing the large glycoside hydrolase family 13 into subfamilies: towards improved functional annotations of α-amylase-related proteins. *Protein Eng., Des. Sel.* **2006**, *19*, 555–562.

(8) Henrissat, B.; Davies, G. Structural and sequence-based classification of glycoside hydrolases. *Curr. Opin. Struct. Biol.* **1997**, *7*, 637–644.

(9) Ly, H. D.; Withers, S. G. Mutagenesis of glycosidases. *Annu. Rev. Biochem.* **1999**, *68*, 487–522.

(10) Liu, Y.; Ma, L.; Chen, W. H.; Wang, B.; Xu, Z. L. Synthesis of xanthone derivatives with extended pi-systems as alpha-glucosidase inhibitors: insight into the probable binding mode. *Bioorg. Med. Chem.* **2007**, *15*, 2810–2814.

(11) Melo, E. B.; Gomes, A. D.; Carvalho, I. Alpha- and beta-glucosidase inhibitors: chemical structure and biological activity. *Tetrahedron* **2006**, *62*, 10277–10302.

(12) Park, H.; Hwang, K. Y.; Kim, Y. H.; Oh, K. H.; Lee, J. Y.; Kim, K. Discovery and biological evaluation of novel alpha-glucosidase inhibitors with in vivo antidiabetic effect. *Bioorg. Med. Chem. Lett.* **2008**, *18*, 3711–3715.

(13) Park, H.; Hwang, K. Y.; Oh, K. H.; Kim, Y. H.; Lee, J. Y.; Kim, K. Discovery of novel alpha-glucosidase inhibitors based on the virtual screening with the homology-modeled protein structure. *Bioorg. Med. Chem.* **2008**, *16*, 284–292.

(14) Park, J. H.; Ko, S.; Park, H. Toward the virtual, screening of alpha-glucosidase inhibitors with the homology-modeled protein structure. *Bull. Korean Chem. Soc.* **2008**, *29*, 921–927.

(15) Pluempanupat, W.; Adisakwattana, S.; Yibchok-Anun, S.; Chavasiri, W. Synthesis of *N*-phenylphthalimide derivatives as alpha-glucosidase inhibitors. *Arch. Pharmacal Res.* **2007**, *30*, 1501–1506.

(16) Zhang, R.; McCarter, J. D.; Braun, C.; Yeung, W.; Brayer, G. D.; Withers, S. G. Synthesis and testing of 2-deoxy-2,2-dihaloglycosides as mechanism-based inhibitors of alpha-glycosidases. *J. Org. Chem.* **2008**, *73*, 3070–3077.

(17) MacGregor, E. A.; Janecek, S.; Svensson, B. Relationship of sequence and structure to specificity in the α-amylase family of enzymes. *Biochim. Biophys. Acta* **2001**, *1546*, 1–20.

(18) Schmidt, D. D.; Frommer, W.; Müller, L.; Junge, B.; Wingender, W.; Truscheit, E. α-Glucosidase inhibitors, new complex oligosaccharides of microbial origin. *Naturwissenschaften* **1977**, *64*, 535–536.

(19) Hanozet, G.; Pircher, H. P.; Vanni, P.; Oesch, B.; Semenza, G. An example of enzyme hysteresis. The slow and tight interaction of some fully competitive inhibitors with small intestinal sucrase. *J. Biol. Chem.* **1981**, *256*, 3703–3711.

(20) Chiasson, J.-L.; Josse, R. G.; Hunt, J. A.; Palmason, C.; Rodger, N. W.; Ross, S. A.; Ryan, E. A.; Tan, M. H.; Wolever, T. M. S. The efficacy of acarbose in the treatment of patients with non-insulin-dependent diabetes-mellitus: a multicenter controlled clinical-trial. *Ann. Intern. Med.* **1994**, *121*, 928–935.

(21) Holman, R. R.; Cull, C. A.; Turner, R. C. A randomized double-blind trial of acarbose in type 2 diabetes shows improved glycemic control over 3 years (UK Prospective Diabetes Study 44). *Diabetes Care* **1999**, *22*, 960–964.

(22) Jenkins, D. J.; Taylor, R. H.; Goff, D. V.; Fielden, H.; Misiewicz, J. J.; Sarson, D. L.; Bloom, S. R.; Alberti, K. G. Scope and specificity of acarbose in slowing carbohydrate-absorption in man. *Diabetes* **1981**, *30*, 951–954.

(23) Taylor, R. H.; Jenkins, D. J.; Barker, H. M.; Fielden, H.; Goff, D. V.; Misiewicz, J. J.; Lee, D. A.; Allen, H. B.; MacDonald, G.; Wallrabe, H. Effect of acarbose on the 24-h blood-glucose profile and pattern of carbohydrate-absorption. *Diabetes Care* **1982**, *5*, 92–96.

(24) Brogard, J. M.; Willemin, B.; Blicklé, J. F.; Lamalle, A. M.; Stahl, A. Alpha-glucosidase inhibitors. A new concept for the treatment of diabetes and reactive hypoglycemias. *Rev. Med. Interne* **1989**, *10*, 365–374.

(25) Kolb, H. C.; Finn, M. G.; Sharpless, K. B. Click chemistry: diverse chemical function from a few good reactions. *Angew. Chem., Int. Ed.* **2001**, *40*, 2004–2021.

(26) Recent reviews: (a) Kolb, H. C.; Finn, M. G.; Sharpless, K. B. The growing impact of click chemistry on drug discovery. *Drug Discovery Today* **2003**, *8*, 1128–1137. (b) Wang, Q.; Chittaboina, S.; Barnhill, H. N. Advances in 1,3-dipolar cycloaddition reaction of azides and alkynes. A prototype of "click" chemistry. *Lett. Org. Chem.* **2005**, *2*, 293–301. (c) Bock, V. D.; Perciaccante, R.; Jansen, T. P.; Hiemstra, H.; Maarseveen, J. H. Click chemistry as a route to cyclic tetrapeptide analogues: synthesis of cyclo-[Pro-Val-(triazole)-Pro-Tyr]. *Org. Lett.* **2006**, *8*, 919–922.

(27) Garcia-Moreno, M. I.; Rodriguez-Lucena, D.; Mellet, C. O.; Fernandez, J. M. G. Pseudoamide-type pyrrolidine and pyrrolizidine glycomimetics and their inhibitory activities against glycosidases. *J. Org. Chem.* **2004**, *69*, 3578–3581.

(28) Rossi, L. L; Basu, A. Glycosidase inhibition by 1-glycosyl-4-phenyl triazoles. *Bioorg. Med. Chem. Lett.* **2005**, *15*, 3596–3599.

(29) Castro, S.; Cherney, E. C.; Snyder, N. L.; Peczuh, M. W. Synthesis of substituted septanosyl-1,2,3-triazoles. *Carbohydr. Res.* **2007**, *342*, 1366–1372.

(30) Rostovtsev, V. V.; Green, L. G.; Fokin, V. V.; Sharpless, K. B. A stepwise Huisgen cycloaddition process: copper (I)-catalyzed regioselective "ligation" of azides and terminal alkynes. *Angew. Chem., Int. Ed.* **2002**, *41*, 2596–2599.

(31) Lu, Y.; Gervay-Hague, J. Synthesis of c-4 and c-7 triazole analogs of zanamivir as multivalent sialic acid containing scaffolds. *Carbohydr. Res.* **2007**, *342*, 1636–1650.

(32) Lee, B. Y.; Park, S. R.; Jeon, H. B.; Kim, K. S. A new solvent system for efficient synthesis of 1,2,3-triazoles. *Tetrahedron Lett.* **2006**, *47*, 5105–5109.

(33) Laskowski, R. A.; MacArthur, M. W.; Moss, D. S.; Thornton, J. M. PROCHECK, a program to check the stereochemical quality of protein structures. *J. Appl. Crystallogr.* **1993**, *26*, 283–291.

(34) Luthy, R.; Bowie, J. U.; Eisenberg, D. Assessment of protein models with 3-dimensional profiles. *Nature* **1992**, *356*, 83–85.

(35) Shirai, T.; Hung, V. S.; Morinaka, K.; Kobayashi, T.; Ito, S. Crystal structure of GH13 alpha-glucosidase GSJ from one of the deepest sea bacteria. *Proteins* **2008**, *73*, 126–133.

(36) Davies, G. J.; Wilson, K. S.; Henrissat, B. Nomenclature for sugar-binding subsites in glucosyl hydrolases. *Biochem. J.* **1997**, *321*, 557–559.

(37) Tschamber, T.; Gessier, F.; Dubost, E.; Newsome, J.; Tarnus, C.; Kohler, J.; Neuburger, M.; Streith, J. Carbohydrate transition state mimics: synthesis of imidazolo-pyrrolidinoses as potential nectrisine surrogates. *Bioorg. Med. Chem.* **2003**, *11*, 3559–3568.

(38) Tomich, C. H.; da Silva, P.; Carvalho, I.; Taft, C. A. Homology modeling and molecular interaction field studies of alpha-glucosidases as a guide to structure-based design of novel proposed anti-HIV inhibitors. *J. Comput.-Aided Mol. Des.* **2005**, *19*, 83–92.

(39) Vocadlo, D.; Davies, J. Mechanistic insights into glycosidase chemistry. *Curr. Opin. Chem. Biol.* **2008**, *12*, 539–555.

(40) Wallace, A. C.; Laskowski, R. A.; Thornton, J. M. Ligplot: a program to generate schematic diagrams of protein−ligand interactions. *Protein Eng.* **1995**, *8*, 127–134.

(41) Gloster, T. M.; Meloncelli, P.; Stick, R. V.; Zechel, D.; Vasella, A.; Davies, G. J. Glycosidase inhibition: an assessment of the binding of 18 putative transition-state mimics. *J. Am. Chem. Soc.* **2007**, *129*, 2345–2354.

(42) Chang, C. E. A.; Chen, W.; Gilson, M. K. Ligand configurational entropy and protein binding. *Proc. Natl. Acad. Sci. U.S.A.* **2007**, *104*, 1534–1539.

(43) Kim, M. J.; Lee, S. B.; Lee, H. S.; Lee, S. Y.; Baek, J. S.; Kim, D.; Moon, T. W.; Robyt, J. F.; Park, K. H. Comparative study of the inhibition of alpha-glucosidase, alpha-amylase, and cyclomaltodextrin glucanosyltransferase by acarbose, isoacarbose, and acarviosine-glucose. *Arch. Biochem. Biophys.* **1999**, *371*, 277–283.

(44) Matsui, T.; Yoshimoto, C.; Osajima, K.; Oki, T.; Osajima, Y. In vitro survey of alfa-glucosidase inhibitory food components. *Biosci., Biotechnol., Biochem.* **1996**, *60*, 2019–2022.

(45) Kanthi, J. M.; Abesundara, T. M.; Kiyoshi, M. Glucosidase inhibitory activity of some Sri Lanka plant extracts, one of which, *Cassia auriculata*, exerts a strong antihyperglycemic effect in rats comparable to the therapeutic drug acarbose. *J. Agric. Food Chem.* **2004**, *52*, 2541–2545.

(46) Sali, A.; Blundell, T. L. Comparative protein modeling by satisfaction of spatial restraints. *J. Mol. Biol.* **1993**, *234*, 779–815.

(47) Watanabe, K.; Hata, Y.; Kizaki, H.; Katsube, Y.; Suzuki, Y. The refined crystal structure of *Bacillus cereus* oligo-1,6-glucosidase at 2.0 angstrom resolution: structural characterization of proline-substitution sites for protein thermostabilization. *J. Mol. Biol.* **1997**, *269*, 142–153.

(48) Notredame, C.; Higgins, D. G.; Heringa, J. T-Coffee: a novel method for fast and accurate multiple sequence alignment. *J. Mol. Biol.* **2000**, *302*, 205–217.

(49) Hooft, R. W.; Vriend, G.; Sander, C.; Abola, E. E. Errors in protein structures. *Nature* **1996**, *381*, 272–272.

(50) Holm, L.; Kääriäinen, S.; Rosenström, P.; Schenkel, A. Searching protein structure databases with DaliLite v.3. *Bioinformatics* **2008**, *24*, 2780–2781.

(51) Thomsen, R.; Christensen, M. H. MolDock: a new technique for high-accuracy molecular docking. *J. Med. Chem.* **2006**, *49*, 3315–3321.

(52) Sobolev, V.; Sorokine, A.; Prilusky, J.; Abola, E. E.; Edelman, M. Automated analysis of interatomic contacts in proteins. *Bioinformatics* **1999**, *15*, 327–332.